ADVANCED HEALTHCARE MATERIALS
www.advhealthmat.de

Continuous Microfiber Wire Mandrel-Less Biofabrication for Soft Tissue Engineering Applications

*Arianna Adamo, Joseph G. Bartolacci, Drake D. Pedersen, Marco G. Traina, Seungil Kim, Antonio Pantano, Giulio Ghersi, Simon C. Watkins, William R. Wagner, Stephen F. Badylak, and Antonio D'Amore**

Suture materials are the most common bioimplants in surgical and clinical practice, playing a crucial role in wound healing and tendon and ligament repair. Despite the assortment available on the market, sutures are still affected by significant disadvantages, including failure in mimicking the mechanical properties of the tissue, excessive fibrosis, and inflammation. This study introduces a mandrel-less electrodeposition apparatus to fabricate continuous microfiber wires of indefinite length. The mandrel-less biofabrication produces wires, potentially used as medical fibers, with different microfiber bundles, that imitate the hierarchical organization of native tissues, and tailored mechanical properties. Microfiber wire morphology and mechanical properties are characterized by scanning electron microscopy, digital image processing, and uniaxial tensile test. Wires are tested in vitro on monocyte/macrophage stimulation and in vivo on a rat surgical wound model. The wires produced by mandrel-less deposition show an increased M2 macrophage phenotype in vitro. The in vivo assessment demonstrates that microfiber wires, compared to the medical fibers currently used, reduce pro-inflammatory macrophage response and preserve their mechanical properties after 30 days of use. These results make this microfiber wire an ideal candidate as a suture material for soft tissue surgery, suggesting a crucial role of microarchitecture in more favorable host response.

1. Introduction

Sutures are the most utilized implants in surgical and clinical practice. Suture materials play an essential role in wound management and repair but are also used for tendons, *chordae tendineae*, or ligament replacement and repair.[1] Ideally, sutures should provide support until the tissue has regained sufficient strength and volume. When this is achieved, the suture material should permanently remain bioinert or fully degrade to prevent further tissue reactions and facilitate endogenous tissue growth.[2] Type, quality of the treated tissues, and the specific clinical setting dictate the suture material's desired physical and biological properties. These factors create a multidimensional design space where time-dependent variables, such as tissue healing rate, add additional levels of complexity.

Technological advancements in the field of biomaterials have introduced into the market an increasing variety of suture materials that are tailored to specific tissue applications. An ideal suture material, both

A. Adamo, J. G. Bartolacci, D. D. Pedersen, M. G. Traina, S. Kim, W. R. Wagner, S. F. Badylak, A. D'Amore
McGowan Institute for Regenerative Medicine
Pittsburgh, PA 15219, USA
E-mail: and78@pitt.edu

A. Adamo, A. D'Amore
Ri. MED Foundation
Palermo 90133, Italy

D. D. Pedersen, W. R. Wagner, S. F. Badylak, A. D'Amore
Department of Bioengineering
University of Pittsburgh
Pittsburgh, PA 15260, USA

M. G. Traina, A. Pantano
Department of Engineering
University of Palermo
Palermo 90133, Italy

G. Ghersi
Department of Biological
Chemical and Pharmaceutical Sciences and Technologies
Palermo 90123, Italy

S. C. Watkins
Department of Cell Biology
University of Pittsburgh School of Medicine
Pittsburgh, PA 15213, USA

W. R. Wagner, S. F. Badylak, A. D'Amore
Department of Surgery
School of Medicine
University of Pittsburgh
Pittsburgh, PA 15260, USA

The ORCID identification number(s) for the author(s) of this article can be found under https://doi.org/10.1002/adhm.202102613

DOI: 10.1002/adhm.202102613

absorbable and not absorbable, is characterized by good handling characteristics, adequate knot security, and tensile strength. It should resist shrinkage, cause minimal tissue reaction, and minimize bacterial proliferation.[3] Bioabsorbable suture materials such as polyglycolic acid (PGA), surgical gut, and polydioxanone (PDS) degrade over time after implantation,[4] with a mechanism mediated by enzymatic digestion, pH variation, and phagocytosis. In contrast, nonbioabsorbable suture materials, including nylon, propylene, polytetrafluoroethylene, are not significantly degraded after implantation and are used when extended mechanical support is required.[5] Monofilament sutures are made of a single strand, resulting in a lower tissue drag and a relatively stronger resistance to microorganisms. However, due to their higher bending stiffness and higher shape memory, crimping can lead to undesirable and premature suture failure. Multifilament sutures are composed of several filaments, usually twisted or braided together. Generally, this feature makes this class of sutures more pliable and flexible than the monofilament, at the cost of a higher suture-tissue coefficient of friction.[3,5]

Inflammation is a crucial component of the host response to suture material implantation.[6] When the inflammatory state becomes chronic, it interferes with wound healing, de novo tissue formation, and increases the risk of infection. Macrophages, among other innate and adaptive immune cells, play an important role in the host response to foreign bodies[7] and, consequently, in the inflammation resolution. Macrophages are a heterogenous cell population, and the different cell functions are controlled by the phenotype. Broadly, polarized macrophages are referred to as M1 or M2 phenotype. M1, or "classically activated," are microbicidal and play a crucial role in cytotoxic host defense. M1 macrophages metabolize arginine and produce high levels of inducible nitric oxide synthase (iNOS), secrete toxic reactive oxygen and nitric oxygen intermediates and inflammatory cytokines (IL-1β, IL-6, and TNFα). The M1 phenotype is typically associated with dense fibrosis and scar tissue formation.[6,7] In contrast, pro-remodeling M2, or "alternatively activated" macrophages, have high levels of scavenger receptors, produce arginase, are involved in polarized Th2 lymphocytes reaction, are able to facilitate tissue repair and constructive remodeling through stem/progenitor cell recruitment and the deposition of extracellular matrix (ECM), have antimicrobial activity, and promote angiogenesis.[8]

Although the cause-effect and the exact mechanisms by which macrophages influence tissue remodeling outcomes remain largely unknown, increases in the number of M2 macrophages and a greater ratio of M2:M1 cells within the site of tissue remodeling were associated with a higher and more favorable remodeling outcome.[7–9]

It has been demonstrated in previous works that a highly organized biomaterial microtopography can promote an anti-inflammatory macrophages phenotype.[10–12] Microfiber-based biomaterials are of great importance for soft tissue engineering and tissue repair surgical strategies, as every form of connective or soft tissue possesses an ECM with a pronounced level of hierarchical and structural organization. Examples include ligaments and tendons,[13] heart valves,[14,15] and nerves.[16]

Fabricating medical fibers with tailored microstructure and mechanical properties will have an enormous impact on tissue healing and function. Microfiber bundles can be obtained via electrodeposition technique: a controlled process that uses electrical forces to fabricate continuous microfibers from a wide variety of materials. Toward this end, several processing approaches have been introduced: Khil et al.,[17] Smit and Sanderson,[18] Teo et al.,[19] and Yousefzadeh et al.[20] utilized a coagulation liquid bath as a preprocessing step to eliminate electrical charges and facilitate fiber bundle formation. Dabirian et al.[21] and Bazbouz and Stylios[22] adopted a moving, solid collecting target with a cylindrical or disk shape. Ali et al.,[23] Afifi et al.,[24] He et al.,[25] Liao et al.,[26] and Richard and Verma[27] used static or rotating funnels with multiple charged nozzles to obtain highly twisted microfiber yarns. Mouthuy et al. used a solid wire as a collecting surface; an elongated electrospun construct is then manually detached from the precursor wire and twisted multiple times to obtain a yarn.[28] These attempts demonstrate the growing interest in this topic and its potential clinical applications. However, processing methods to produce continuous, microfiber wire with indefinite length remain at an early stage. Most importantly, little effort has been made to elucidate the role of a tailored-to-the-needs microfiber scaffold in the specific context of suture material and tissue healing.

In this work, poly(ester urethane) urea (PEUU), continuous microfiber wires with tunable mechanics and ultrastructure have been fabricated by a novel mandrel-less apparatus. The microfiber PEUU wires were characterized by an integrated set of in silico, in vitro, and in vivo experiments. The mechanism of fiber electrodeposition without a solid collecting mandrel was studied in silico by simulating the 3D voltage distribution induced by the electrodes. The in vitro models focused on elucidating the impact of the ultrastructural cues on macrophage activation switching. PEUU degradation products from cast and microfiber layers fabrications were used to treat bone marrow-derived macrophages (BMMs). BMMs were also seeded in direct contact with PEUU cast and microfiber layers and wires to study the immunomodulatory characteristics of the substrate ultrastructure in a controlled environment. The macrophage phenotype transition was evaluated through immunolabeling and immunoblotting. The response observed in the in vitro experiments was further studied in vivo, where PEUU microfiber wires have been implanted as suture material in a rat surgical wound model and compared to commercially available sutures, including PGA, PDS, and polypropylene (PPL). After 1 month, mechanical, histological, and immunological evaluation of explants was performed.

Overall, results from this in silico–in vitro–in vivo integrated approach indicate that PEUU microfiber, generated with controlled ultrastructure and mechanics, induces macrophage activation toward a pro-remodeling, anti-inflammatory (M2-like) phenotype. Specifically, the in vitro experiments showed that the macrophage phenotype switch to the M2-like was promoted by the microfiber scaffold ultrastructure. The results obtained

W. R. Wagner
Department of Chemical Engineering
University of Pittsburgh
Pittsburgh, PA 15260, USA
A. D'Amore
Clinical Translational Science Institute
University of Pittsburgh
Pittsburgh, PA 15260, USA

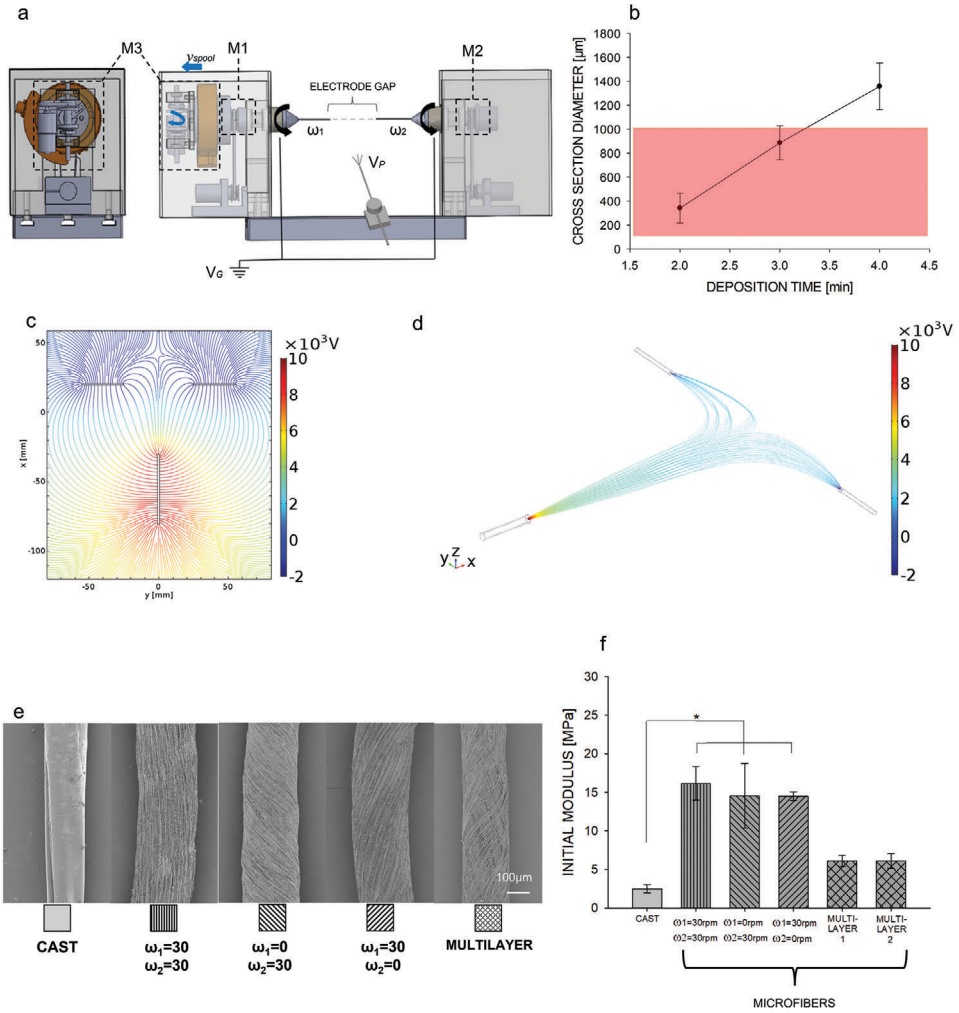

Figure 1. Mandrel-less fabrication of microfiber-based wire: apparatus and processing method. a) Schematic of the prototype of the apparatus developed in this study and its processing variables. Two high voltage generators control the negative voltage of the two electrodes (V_G) and the positive voltage of the polymer source (V_P). Slits on the base and a moving arm allow modifications of the electrode gap and the polymer-target gap. Motor 1 (M1) in tower 1 controls the rotation of electrode 1 (ω_1), Motor 2 (M2) in tower 2 controls the rotation (ω_2) of electrode 2, the two electrodes spin around a common axis. Tower 1 is also equipped with a third motor (M3) responsible for the linear velocity and motion of the spool (υ_{spool}). This mechanism allows the continuous collection of the forming wire to achieve any prescribed construct length. The polymer spinneret is positioned in between the two electrodes. A Harvard apparatus controls the polymer flow rate. A balance between the polymer mass introduced in the system via electrodeposition and the polymer mass accumulated on the spool allows for the continuous production of the microfiber-based rope. b) Diameter versus fiber deposition time characteristic for the following fabrication variables: V_P: 10 kV, V_G: −2 kV, flow rate: 3 mL h^{-1}, polymer-electrode gap: 5 cm, electrode gap: 5 cm, $\omega_1 = \omega_2$: 30 rpm. Five samples were fabricated for each time point: 2, 3, and 4 min. The red area indicates the diameter range of interest for suture materials available on the market. Electric field COMSOL model: c) 2D FEM analysis. Electric field lines symmetrically split as they depart from the polymer source and direct toward the collecting electrodes. d) 3D FEM analysis. Electric field lines in isometric view. e) SEM analysis at 100X magnification. The ratio between the rotational speeds of the two electrodes dictates different fiber arrangements. Multilayer composite ropes can be formed by combining two or more fiber deposition configurations in sequence. Fabrication variables utilized for all of the groups: V_P: 10 kV, V_G: −2 kV; flow rate: 3 mL h^{-1}; polymer-electrodes gap: 5 cm; electrode gap: 5 cm. Fabrication time: 3 min (see Table 1 for more details). f) PEUU cast and microfiber wire initial moduli comparison. Uniaxial tensile test results show the capacity to modify the mechanical properties of the wires by changing the fiber arrangement while delivering the identical polymer mass during the deposition process (* = $p < 0.05$).

in vitro were confirmed by the in vivo model. Rats implanted with a tailored PEUU microfiber suture wires showed a higher M2/M1 ratio and equivalent collagen content within the scar area compared to an analog healthy skin area of the control group. The PEUU microfiber wires mechanical properties remained unchanged after 30 days of implantation, and the initial modulus was comparable to the one measured for the treated native tissue.

2. Results

2.1. Analysis of the Electric Field

A finite element simulation of the electric field generated during the mandrel-less fabrication was conducted in 2D and 3D (**Figure 1**c,d, respectively) using COMSOL Multiphysics. The

Table 1. Microfiber wire fabrication parameters.

	Mandrel rotation [rpm]	Deposition time [min]	Total deposition time [min]
	$\omega_1 = 30 - \omega_2 = 30$	3	3
	$\omega_1 = 0 - \omega_2 = 30$	3	3
	$\omega_1 = 30 - \omega_2 = 0$	3	3
Multilayer 1	$\omega_1 = 30 - \omega_2 = 30$ $\omega_1 = 0 - \omega_2 = 30$ $\omega_1 = 30 - \omega_2 = 0$	111	3
Multilayer 2	$\omega_1 = 0 - \omega_2 = 30$ $\omega_1 = 30 - \omega_2 = 0$ $\omega_1 = 30 - \omega_2 = 30$	111	3

electric field model prediction demonstrates how the field distribution bifurcates in the proximity of the negatively charged electrodes. According to the experimental observation, the positively charged microfiber jet approaches the electrodes then reaches the edge of the nearest electrode while the other segment of the microfiber jet deposits to the other electrode edge. This initial part of the process creates the first polymeric deposition between the two electrodes. Once the first fiber connects the two electrodes, the rest of the deposition continues while the rotating electrodes transmit motion to the accumulating fibers. The COMSOL model consistently identifies the warm and cold regions of the electric field in proximity to the electrode edges, highlighting trajectories of higher probability for the fiber flocculation. Additional modeling results can be found in Figure S2 in the Supporting Information.

2.2. Wire Diameter Range and Mechanical Response

The microfiber suture wire cross-section diameter versus the deposition time characteristic is shown in Figure 1b. The area highlighted in red shows the diameter range for suture wires that are currently available on the market. Three fabrication times were considered to characterize the diameter versus time linear relationship; $n = 5$ independent fabrications were completed for each time point with variables described in the Experimental Section and rotational speed of 30 rpm for both of the electrodes (see *Poly(Esther Urethane)Urea (PEUU) microfiber-based suture wire fabrication* section). For each sample, diameters were measured from five random locations using a brightfield microscope. An R^2 of 0.99 confirmed the linear nature of the diameter versus time curve. Uniaxial mechanical properties of different microfiber wire fiber depositions are presented in Figure 1f, $n = 4$ independent fabrications were conducted for each group (fabrication parameters are reported in **Table 1**). Figure 1f shows statistically significant changes in initial modulus induced by simply modifying the fiber arrangement while delivering the identical polymer mass during the deposition process. Additional information about the physical characteristics of microfiber wires and their comparison with results previously obtained in literature is shown in Table S1 in the Supporting Information.

2.3. Scanning Electron Microscopy (SEM) and Scaffold Surface Characterization

Analysis of microfiber deposition has been conducted with SEM and digital image analysis for all of the scaffold groups ($n = 7$ per group) considered in the study. As expected, SEM qualitative evaluation showed that different microfiber arrangements, in terms of the preferential direction of the alignment, can be achieved by changing the electrode rotational direction (**Figures** 1e, **2**a, and Figure S3, Supporting Information). A custom-made MATLAB algorithm[29] was utilized to quantitatively characterize the microfiber wire surface topology. Results showed that the rotational velocity of the electrodes affects the fiber orientation angle (Figure 2c) without altering fiber diameter (Figure 2b), pore size (Figure 2d), and porosity (Figure 2e). This feature allows for decoupling the design of fiber micro-topology from fiber network alignment at the mesoscale.

2.4. In Vitro Macrophage Response to the PEUU Layer Degradation Products

The phenotypic profile of murine BMMs was determined by immunolabeling via the expression of: F4/80, a pan-macrophage marker; iNOS, an M1-like pro-inflammatory marker; or Arginase1 and Fizz1, M2-like anti-inflammatory markers (**Figure 3**a). Known factors that are promoters of pro-inflammatory (LPS and IFN-γ) or anti-inflammatory (IL-4) phenotypes were included as controls. Exposure of macrophages to PEUU microfiber degradation product with a 1:50 dilution showed a decrease in the number of cells expressing iNOS ($p < 0.05$) when compared to the other treatments (Figure 3c). The PEUU microfiber degradation products, with a 1:10 dilution, increased ($p < 0.05$) the percentage of cells expressing Fizz1 when compared to the PEUU microfiber degradation products at 1:50. PEUU cast degradation products at 1:50 also showed a statistically significant decrease in the number of cells expressing the same marker compared to the other treatments (Figure 3d).

2.5. Effect of Substrate Microarchitecture to Macrophage Polarization In Vitro

The effect of PEUU layers and PEUU microfiber wires on BMMs protein expression was determined by Western blot and immunolabeling. Specifically, the expression of M1-like marker iNOS and M2-like markers Arginase1 and Fizz1 was evaluated. When BMMs were seeded on PEUU microfiber and cast layers, they induced the expression of both Arginase 1 and iNOS proteins (**Figure 4**a,b). However, BMMs seeded PEUU microfiber layer showed a significantly higher Arginase1 expression when compared to the BMMs seeded PEUU cast ($p < 0.05$) (Figure 4a).

Western blot results obtained on PEUU layers were further corroborated by the immunolabeling experiment conducted on PEUU microfiber wires. Both the PEUU layer and PEUU wire scaffold types are 3D in nature. However, while identical at the microfiber level, the microfiber wires have a suture-like tubular morphology at the macroscale. Qualitative analysis of the BMMs response to the interaction with PEUU microfiber wires is presented in Figure 4d. The percentage of positive macrophage for

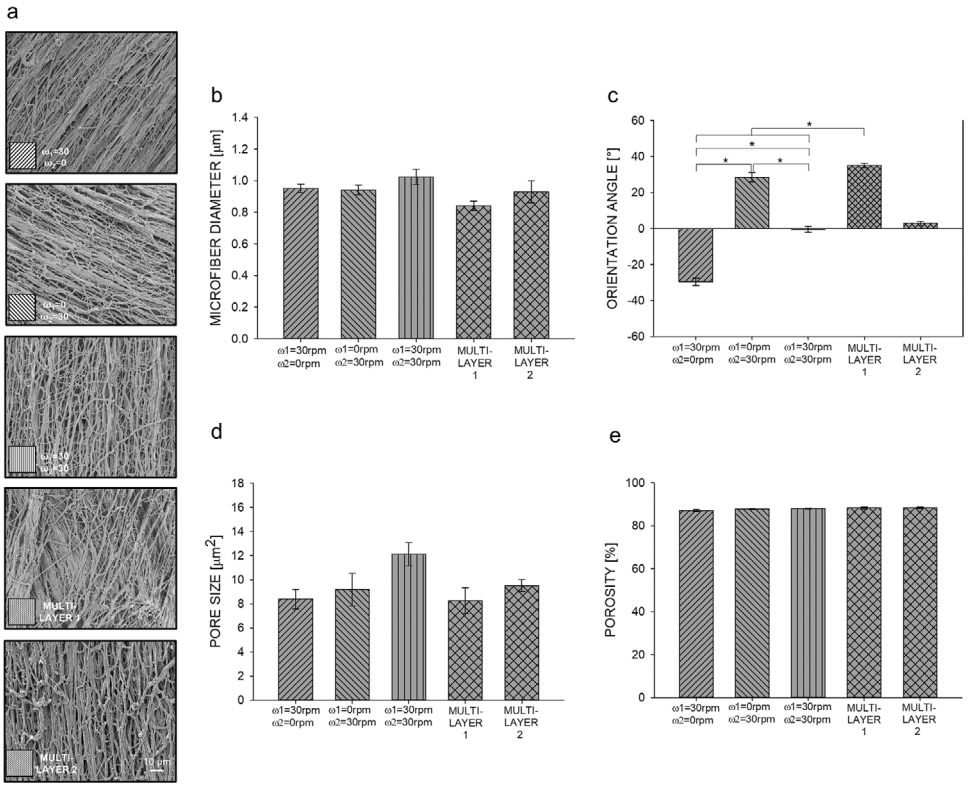

Figure 2. Scanning electron microscopy and quantitative topological analysis of the polymeric suture wire. a) SEM analysis at 1000X magnification. 35 images, 7 per group, were collected to characterize the wire ultrastructure and show how it can be affected by the electrode kinematics. b) Microfiber diameter. c) Main orientation angle for the fiber network. d) Pore size and e) bulk porosity. Quantitative analysis showed that electrodes' relative velocity only affects the main direction of the fibers while the other independent structural variables are left unmodified (* = $p < 0.05$).

iNOS and Fizz was measured using CellProfiler. The number of macrophages expressing Fizz1 was significantly higher when compared to the number of macrophages expressing iNOS (Figure 4c). Further details about the topological characterization of PEUU microfiber layers and PEUU microfiber wires are shown in Figure S4 in the Supporting Information.

2.6. Gross Healing Evaluation and Histological Assessment of Collagen Remodeling

The wound healing progression in the different groups was visually inspected and recorded on days 0, 14, and 30 (**Figure 5**). Despite the difference in structures and sizes, each suture wire formed a stable knot. Macroscopically, the evaluation of surgical wounds did not show any difference; however, 30 days after surgery, the PGA suture material had completely degraded while the suture wires were still present in the other groups. Sagittal cross-sections of the tissue explants were stained with Masson's trichrome and used to quantify the collagen fraction within the sample. The histological sections showed differences between groups in terms of cellular infiltration, adipose tissue, collagen deposition, and the presence of hair follicles (**Figure 6**a). The explants qualitative inspection was coupled with quantitative measurements. Images were cropped among the area of interest, collagen spatial density underneath the wound was calculated and compared to an equivalent area of healthy rat skin. While the gross observation showed complete epithelialization for all of the groups at day 30, the results of the quantitative analysis showed that collagen density was significantly lower in the PGA and PDS groups when compared to the healthy skin group ($p < 0.05$) (Figure 6b). Additional images of histological sections are provided in Figure S5 in the Supporting Information.

2.7. Assessment of the Host Response

The spatial distribution of macrophages within the wound section was characterized by immunolabeling. The co-expression of the pan-macrophage cell-surface marker CD11b with the M1-like pro-inflammatory marker iNOS or with the M2-like anti-inflammatory marker Fizz1 is shown in **Figure 7**a. As expected, after 30 days, all the suture materials induced inflammatory response. The characterization of M2-like macrophages, identified as Fizz1+ cells, showed significant differences between the groups. Statistical analysis of the M2-like macrophage population showed differences ($p < 0.05$) between PEUU microfiber versus healthy skin, PDS, and PEUU cast, as indicated in Figure 7c. Quantification of M1-like macrophages, identified as iNOS+ cells, is presented in Figure 7d. The differences observed in M2 and M1 macrophage subpopulations among the groups were further described by the ratio of M2-like:M1-like macrophages and are provided in Figure 7b.

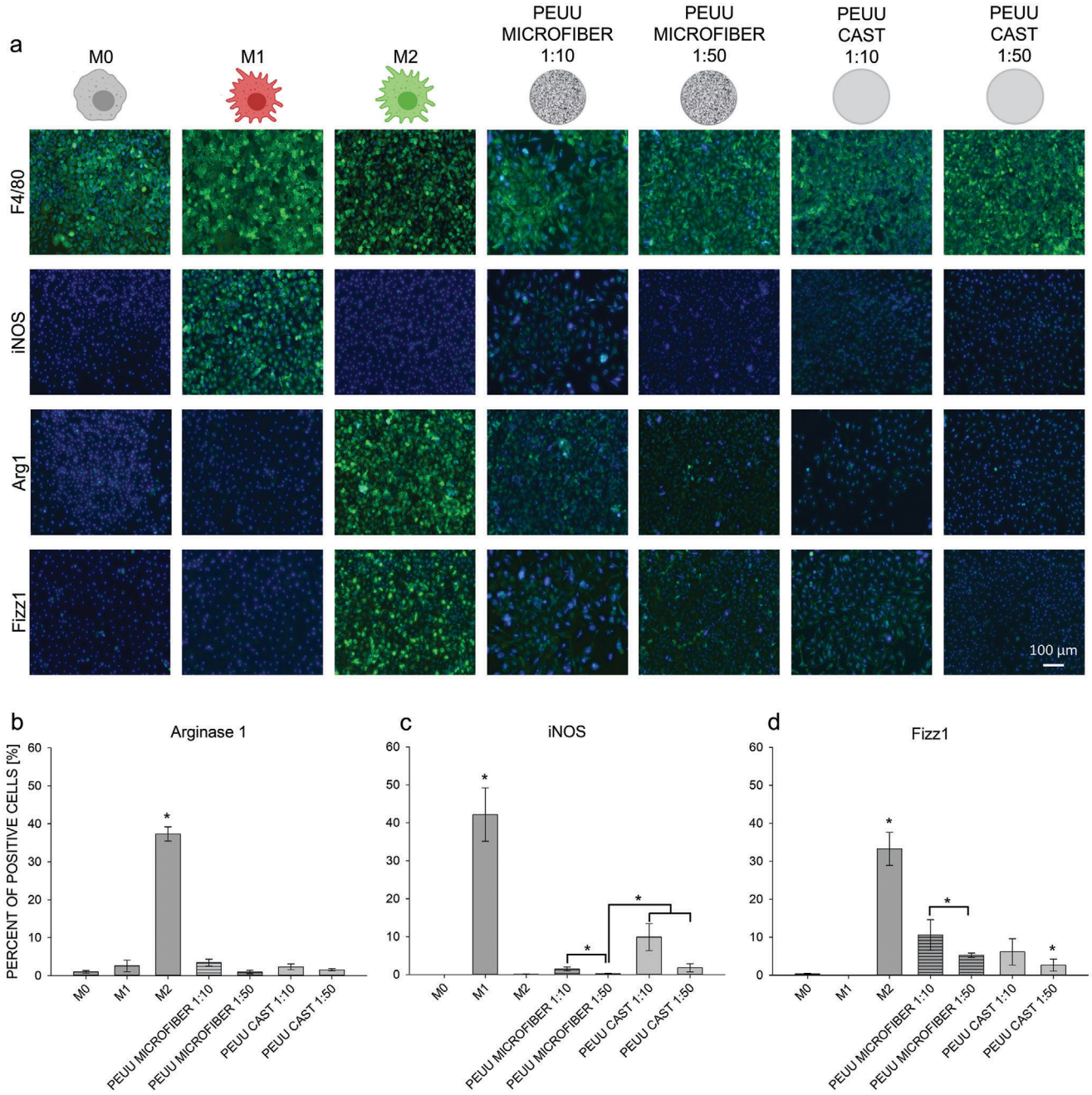

Figure 3. In vitro assessment of macrophage response to PEUU degradation products. a) Activation of markers associated with pro-inflammatory (iNOS) and anti-inflammatory (Fizz1 and Arginase1) phenotype was evaluated by immunolabeling. A general marker of macrophages (F4/80) was used. Known factors that are promoters of pro-inflammatory (100 ng mL^{-1} LPS and 20 ng mL^{-1} IFN-γ) or anti-inflammatory (20 ng mL^{-1} IL-4) phenotypes were included as controls. b–d) Quantitative analysis of the macrophages' response to PEUU degradation products. Images were processed using Cell Profiler image analysis software. Differences between stimuli for each marker were evaluated using a nonparametric ANOVA test (* = $p < 0.001$).

2.8. Pre- and Post-Implant Uniaxial Mechanical Properties of Suture Wires

The initial modulus of pre- and post-implant suture wires is shown in **Figure 8**a. The statistical analysis detected significant changes of initial modulus between the pre- and post-implant of the PEUU cast, PPL, PGA groups. As expected, the most radical change was observed for the PGA suture that was totally re-absorbed at the end of the experiment and therefore was not tested. Pre-implant of PPL, PGA, PDS groups showed statistically significant differences compared to the rat skin control group. For the post-implant evaluation, only the PEUU cast was different than the rat skin control. **Figure 9**b shows the strain at break of pre- and post-implant suture wires. Pre-implant PEUU

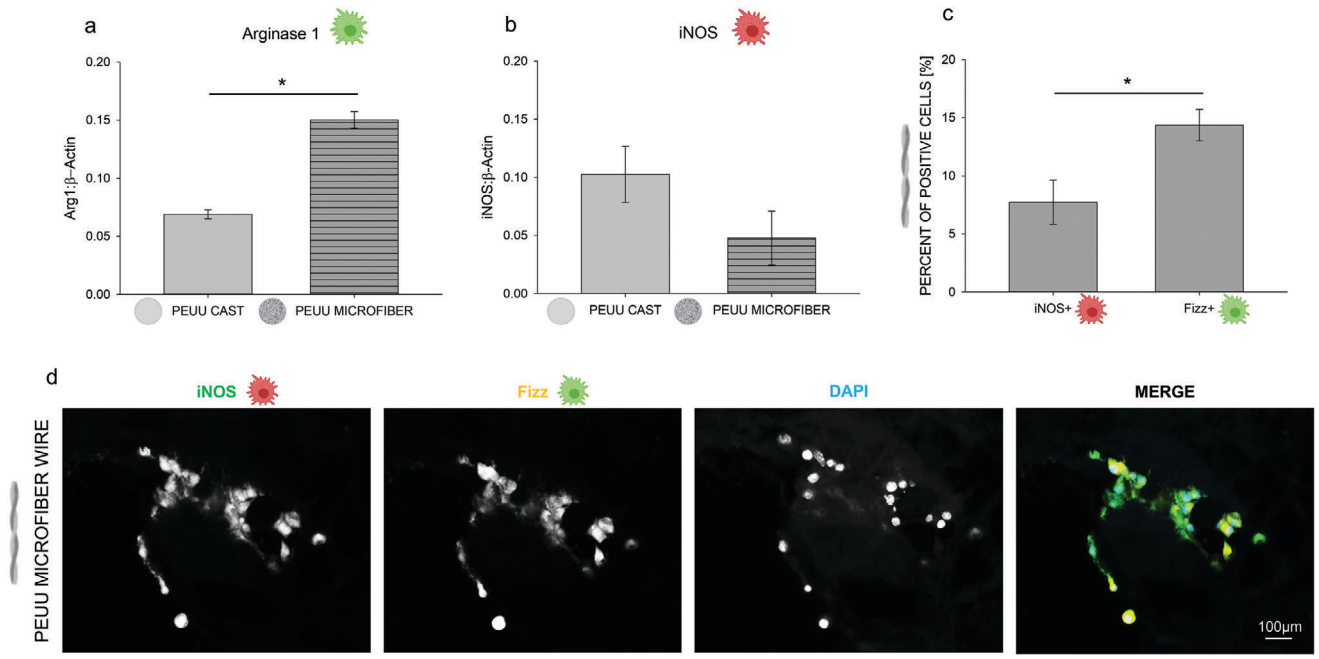

Figure 4. In vitro assessment of macrophage response to PEUU layer and wire scaffold morphologies a) Arginase1 and b) iNOS normalized to the β-actin (* = $p < 0.05$). c) PEUU microfiber wire immunolabeling quantitative analysis: pro and anti-inflammatory protein expression, iNOS, and Fizz, normalized to the total number of cell nuclei (* = $p < 0.05$). d) PEUU microfiber wire immunolabeling qualitative evaluation.

microfiber and PPL groups showed significant differences versus the rat skin control group. The ultimate tensile strength of the different groups is provided in Figure 8c. It shows significant differences between the pre-implant PPL, PGA, and pre- and post-PDS groups when compared to the rat skin control group. The PEUU cast group was the only one characterized by a significant post-implantation increase of the ultimate tensile strength.

2.9. Biaxial Mechanical Characterization of Rat Skin

Equi-membrane tension biaxial test protocol was performed to characterize the in-plane mechanics of explanted tissue in the region of the sutured area at 30 days from the implantation. As reported in Figure 9, all groups showed greater stiffness over the longitudinal direction (craniocaudal) when compared to the circumferential direction. Statistical analysis showed that different suture materials did not induce differences between the groups in terms of macroscale biaxial mechanics compared to the healthy rat skin control group.

3. Discussion

The development of bioimplants, including suture materials, that are more capable of mimicking the structure and function of native ECM is increasingly gaining attention.[1,31] Microenvironmental cues, including surface or volume topographical features (e.g., pore size, pore or fiber interconnectivity, pore aspect ratio, bulk porosity, fiber diameter, orientation, and alignment), play a pivotal role in modulating cell response, inflammation, and de novo tissue formation.[32,33] However, while progress has been made in understanding these effects on somatic cells, the impact of the microenvironment on the immune cell response is still ill-defined. In particular, macrophages are among the first cells to respond to biomaterials. Their initial interaction with the substrate and their polarization to M1-like pro-inflammatory or M2-like anti-inflammatory phenotype are central factors for bioimplant clinical outcomes.[7,8,33]

Suture materials are the most common implants used daily in clinical and surgical practice. Despite the broad spectrum of suture materials available on the market, current research efforts are still focused on developing suture materials with improved physical, mechanical, and microenvironmental properties in an effort to augment customization and enhance functional outcomes.[34]

Microfiber-based materials can provide a mechanical and structural microenvironment able to mimic the hierarchical structure of native connective tissue. This feature is generally more favorable to constructive remodeling than amorphous or nonfibrillar morphologies.[11,35] This study speculates that the bioinspired, microfiber substrate approach can be successfully translated to suture materials that, while not meant to remodel, may suffer from undesired, excessive fibrotic response[32,36] and prolonged inflammation.[37,38]

Microfiber wires can also be adopted for tendon and ligament replacement in orthopedic surgery, *chordae tendineae* replacement and repair in cardiac surgery, and as suture materials for soft tissue injuries. While pre-clinical models support the potential of microfiber-based planar scaffolds for tendon and ligament engineering,[39] limited attempts have been made in

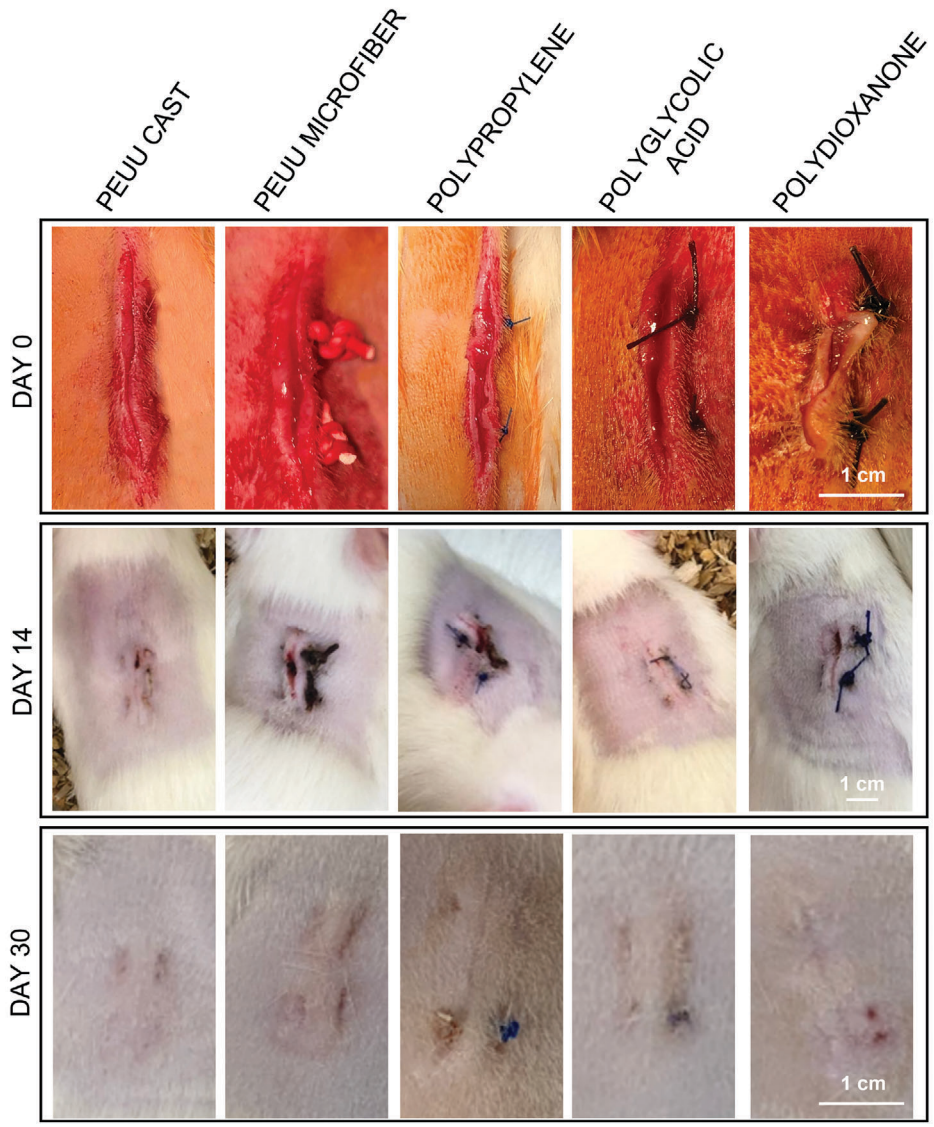

Figure 5. Visual inspection of the wound site over time up to 30 days from the implantation. Visual inspection of wound site to assess suture healing at day 0, day 14, and day 30 after the animal sacrifice.

duplicating the architecture of these anatomical structures at both the macro- and microscales.[13,40] In addition to the suture material applications discussed in this study, recent efforts are focused on modeling[41] and characterizing[42] atrioventricular heart valve chordal apparatus as well as improving *chordae* repair procedures.[43] These studies further reinforce the interest in developing engineered microfiber structures with circular cross-sections in the 570–1270 µm diameter range and a length ≥11 mm.[44]

Due to its versatility and low cost, electrodeposition is one of the most common processing techniques utilized to obtain microfibers. Microfiber-based bioimplants, including engineered heart valves,[14] blood vessels,[45] skin,[46] and bones,[47] fabricated by electrodeposition, can allow for adequate cell infiltration, mechanical support, and biomimicry of native tissue microstructure.

However, despite these recognized advantages, only a limited fraction of studies have reported processing methods for microfiber wire with circular cross-sections and unlimited construct length. These two geometric characteristics are relevant for the production of suture materials, and while they may appear conceptually trivial, they pose significant processing challenges. Microfiber bundles can be generated using a wide range of collectors that differ in geometry, kinematic, and even physical state. These include: liquid surfaces,[17,19,20,48] static or rotating funnels,[23,24,26,27,49] disks,[22] moving targets as cylinders or rollers,[50] stainless steel wires,[28] or multipolar field sources.[21] Nevertheless, these techniques have shown fundamental limitations in controlling scaffold structure–function and reproducibility. Most importantly, from a translational science perspective, only a modest portion of these studies has addressed in vitro and in vivo performances of the engineered device.

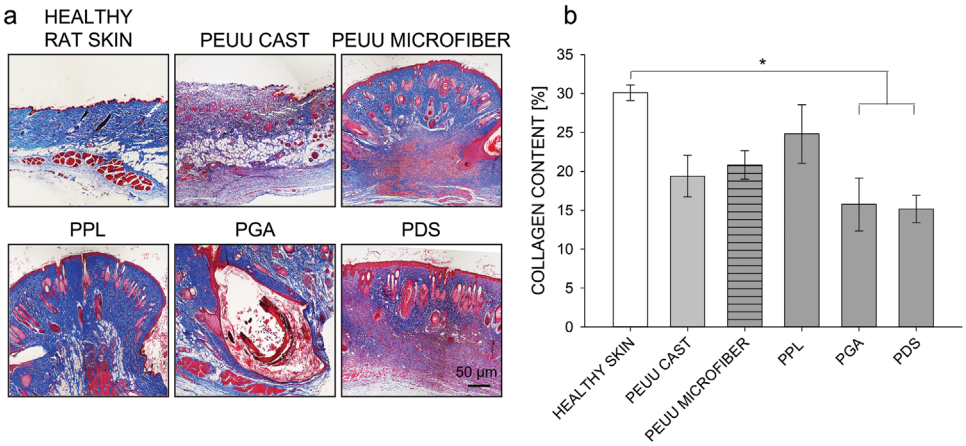

Figure 6. In vivo collagen synthesis and remodeling within the wound site. a) Qualitative histological evaluation via Masson's trichrome staining was conducted to evaluate de novo tissue formation, cellular infiltration, and scar formation. Explants at 30 days from the implantation were compared to healthy rat tissue. b) Quantitative histological evaluation. Collagen quantity in the proximity of the wound site was calculated with a digital image analysis method we previously validated and utilized to assess in vitro collagen synthesis or fibrosis.[30] PPL, PEUU cast, and microfiber wire explants were associated with collagen content comparable to the healthy skin control (* = $p < 0.05$).

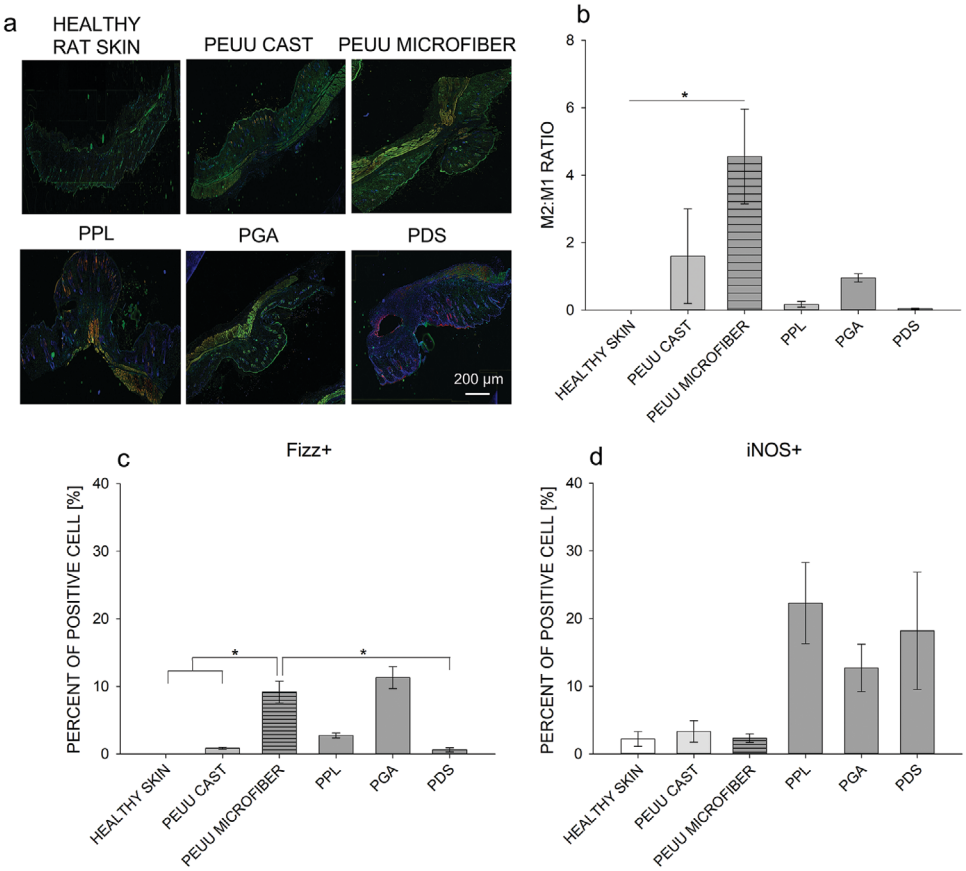

Figure 7. In vivo assessment of macrophage response. a) Representative images utilized for the qualitative and quantitative host response evaluation. Anti-iNOS (M1 marker) and anti-Fizz1 (M2 marker) were used to evaluate macrophage phenotype within the 30 day explants. Images were processed using Cell Profiler image analysis software. Healthy rat skin was adopted as the control group. b) Quantification of M2-like:M1-like macrophage ratio. The ratio of M2-like:M1-like was calculated within a tissue zone centered on the sutured area. c,d) Bar charts show the percentage of Fizz+ and iNOS+ cells (* = $p < 0.05$).

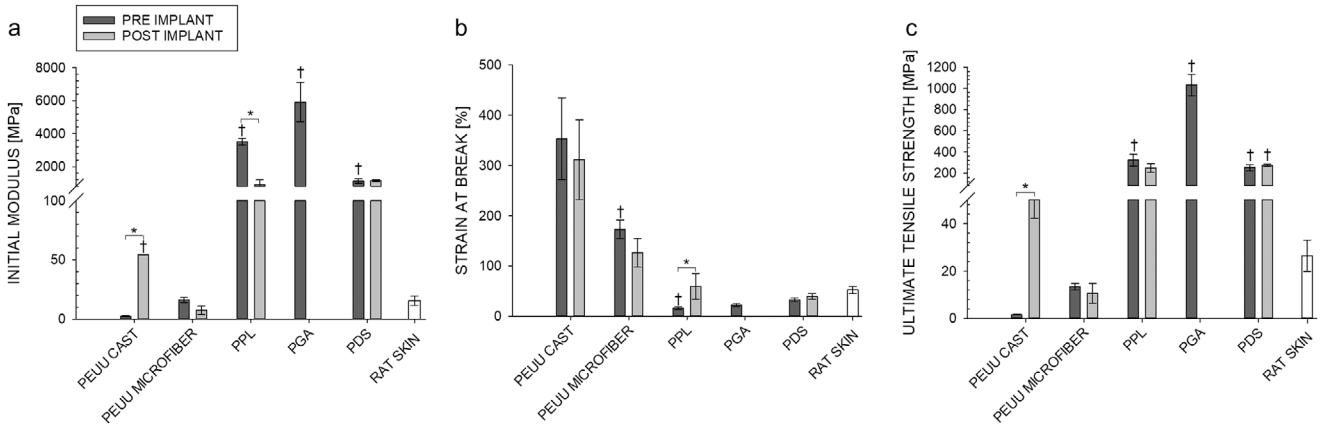

Figure 8. Pre- and post-implant tensile properties. a) Initial tensile moduli comparison before and 30 days after implantation showing differences between the groups and differences dictated by the remodeling or the degradation of the suture material. Healthy rat skin was utilized as the control group. The analysis showed significant differences between the pre-implant PEUU cast, PPL, PGA, and PDS groups versus the rat skin control group. In contrast, results showed no significant differences between PEUU microfiber and the rat skin control group (* = $p < 0.05$). This suggests a reduced mechanical mismatch between the native tissue and the PEUU microfiber wire. b) Strain at break group comparison. c) Ultimate tensile strength group comparison. Similar to the initial moduli, pre-implant PPL, PGA, and PDS groups had significantly greater ultimate tensile strength than the one calculated for the rat skin control group (* = $p < 0.05$).

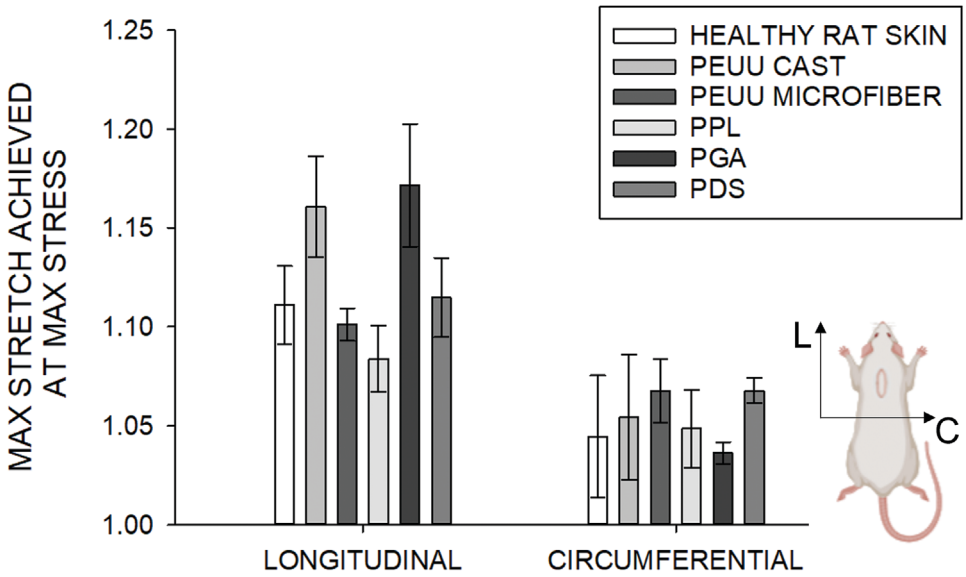

Figure 9. Pre- and post-implant in plane mechanical response under equi-stress biaxial conditions. After 30 days, the rats were sacrificed, and the dorsal skin was collected for mechanical evaluations. The biaxial test was performed on a custom-built planar biaxial stretching system. Healthy rat skin was used as a control to highlight similarities or differences for the in-plane mechanical response of the explants that could have been a source of long-term mechanical mismatch. Results showed no differences among groups; the wound site maintained its natural anisotropy with the circumferential direction stiffer than the longitudinal.

The present work introduced a mandrel-less electrodeposition methodology and apparatus that allows the fabrication of microfiber wires, from either degradable or nondegradable polymers, with indefinite construct, circular cross-section, and improved control on microarchitecture (Figure 1a and Figure S1, Supporting Information).

The wire fabrication starts when the polymeric microfibers are collected in a gap between two facing electrodes and then macroscopically span from one electrode to the other. The electrodes are connected to two motors with variable speed rotation, and a take-up unit is responsible for collecting the yarn. The continuous microfiber wire fabrication, previously introduced from other groups, is augmented by some advantages and factors of novelties. First, the process is automatic and does not require the manual interaction of an expert operator, such as stretching, annealing, or twisting the wires, all technical aspects of the processing that can be a source of experimental variability. Second, the rotation of the mandrels ensures the regularity of the yarn shape and tunes the microfiber architecture. Moreover, this technique allows the production of wires with a wide range of diameters,

from 250 to 1200 μm, which can be used as suture materials and as tissue surrogates for tendon and ligaments repair.

In this report, the mandrel-less apparatus and fabrication characterization have been reported.

SEM analysis and digital image analysis were conducted to determine the wire microarchitecture and how the motor kinematics can affect it (Figures 1e, 2a, and Figures 3 and 4, Supporting Information). The SEM micrographs of the wire surface were analyzed using a custom-made MATLAB algorithm[29] for detailed quantitative topology characterization. The detected main direction of fiber alignment was consistent with the prescribed kinematics (Figure 1e and Figure S3, Supporting Information): $-29.6° \pm 5.4°$ for $\omega_1 = 30$ rpm and $\omega_2 = 0$ rpm, $+28.4° \pm 6.9°$ for $\omega_1 = 0$ and $\omega_2 = 30$ rpm, $-0.4° \pm 4.3°$ for $\omega_1 = 30$ and $\omega_2 = 30$ rpm (Figure 2c).

While other processing apparatuses comprise rotating electrodes,[21–24] this study is the first that introduces the notion of electrode relative velocity as a processing parameter able to tune the main direction of alignment of the microfiber within the wire while maintaining a circular cross-section at the macroscale. Importantly, microfiber diameter, pore size, and porosity remained constant among the groups (Figure 2b,d,e). These results demonstrated that the fiber angle arrangement is an independent variable that can be imposed by changing the electrode rotational velocities without impacting other critical structural features. Further characterization of the fabrication system and method will be necessary to investigate better the design space in terms of fiber diameter, pore size, and porosity ranges that can be achieved. However, based on[51] and our previous work,[14] it is expected that varying voltage gap, electrode-injector gap, and polymer/solvent ratio will allow modifying of at least one (0.1–1 μm) and two orders (1–10 μm) of magnitude of the fiber diameter and the pore size, respectively.

These two structural parameters, in particular, play an essential role in cell–scaffold interaction, including cell proliferation, infiltration,[52] and macrophage polarization.[53] The same quantitative approach was applied at the macroscopic scale length by characterizing the microfiber wire cross-section diameter versus deposition time relationship (Figure 1b). Results showed that the wire diameter is a linear function of the deposition time. Unlike polymer deposition layout based on facing blades[54] or over two static cones,[55] the rotation of the electrodes allows one to obtain circular cross-sections. Furthermore, only a few processing technologies for polymeric microfiber allow for wire diameter tunability that often remains limited in the maximum wire size. In contrast, the wire diameter values we reported cover the full range of interest for commercially available suture materials (100–1000 μm).[56] To elucidate how different microarchitectures affect the wire mechanical properties, uniaxial tensile test was performed.

The PEUU cast wires were used as the control group, while five different microfiber configurations, including mono and multilayers, were evaluated (fabrication variables shown in Table 1). While identical polymer mass was delivered during the deposition process of the different groups, changes in the yarn microarchitecture resulted in significant variations in the uniaxial mechanical properties of the wires. More specifically, this processing strategy permits modifying the initial elastic modulus by a factor of 3 while using the same polymer chemistry and mass as shown in Figure 1f.

Macrophage phenotypic switch is a critical determinant of the host response.[8,32,33] Accordingly, the present work hypothesizes that suture microstructure and mechanical properties can play a role in macrophage polarization. This report utilizes a set of in vitro and in vivo experiments to investigate the potential effects of topographical cues on macrophage phenotype. While not applied to the specific case of suture materials, this hypothesis is supported by a number of studies[12,37] that have shown how scaffold morphology at the micro- and mesoscale, microfiber thickness, chemical composition, and mechanical properties affect the macrophagic switch. Appropriate de novo collagen synthesis and remodeling are also important metrics for evaluating host tissue response to biomaterials,[8,32] and they were investigated in this study.

The PEUU cast degradation products promoted a higher proinflammatory effect showing a significantly higher iNOS level for the [1:10] group (Figure 3c). At the same time, the [1:10] PEUU microfiber degradation products produced the highest values of Fizz1 (Figure 3d). This is commonly associated with the M2-like macrophage phenotype. M0, M1, and M2 controls showed results in agreement with previous models utilized to evaluate host response to bioimplants.[9,57]

This is the first study documenting the in vitro response of macrophages to microstructured versus cast (nonstructured) PEUU scaffold degradation products (**Figure 10**a). While it appears logical and can be speculated that differences in microstructure affect the degradation rate,[53] understanding this effect may require further investigation and can be considered one of the limitations of this study.

However, one of the central questions for our research hypothesis was whether or not direct exposure to an organized scaffold microstructure could elicit measurable effects in terms of the M1–M2 switch in the specific context of engineered suture material.

To determine if the direct contact between macrophages and scaffold microstructure could determine the macrophagic switch, BMMs were seeded directly onto a PEUU microfiber and cast layers and onto PEUU microfiber wires (Figure 10b). The expression of Arginase1 and iNOS was evaluated on BMMs seeded onto PEUU layers via immunoblotting, while Fizz and iNOS expression was assessed on BMMs seeded on PEUU microfiber wires via immunolabeling. Consistently with the results obtained within the previous experiment, which strictly focused on the degradation products without direct scaffold–cell interaction, when BMMs were seeded onto the PEUU microfiber flat layers, a significantly higher expression of Arginase 1, M2-like phenotype marker, was observed (Figure 4a). Comparable significant differences were also observed for macrophages seeded onto PEUU microfiber wires. BMMs showed an increase in Fizz expression compared to iNOS (Figure 4c). Due to the unique and specific nature of this work, which focuses on topological cues and suture material, a direct comparison with a previously published study is not available. Yet, our results on the macrophagic switch are consistent with other reported findings, suggesting that microfiber scaffolds, both layers and wires, evocate an M2-like anti-inflammatory reaction in macrophages, supporting the

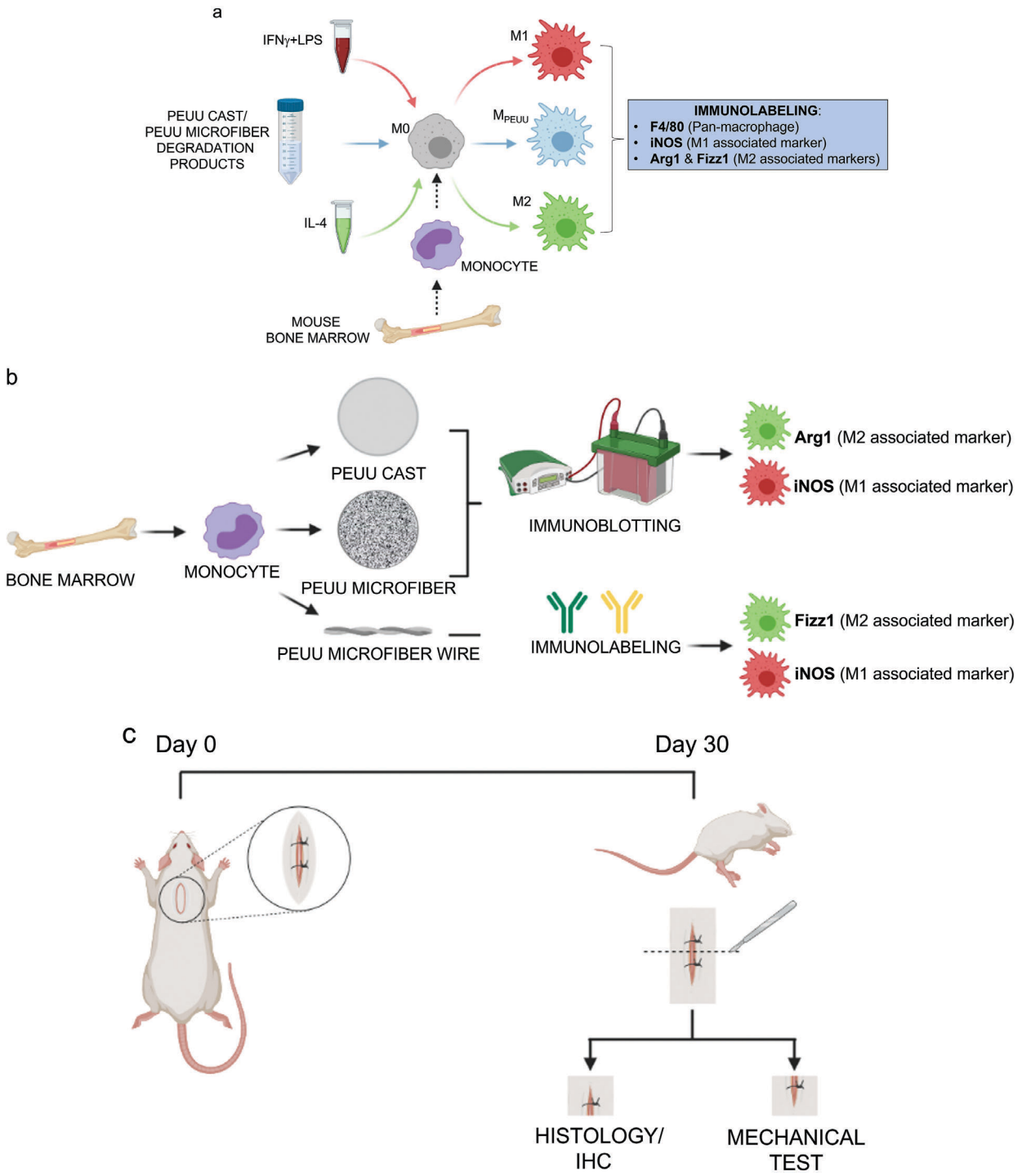

Figure 10. Visual abstracts of the in vitro assessment for the macrophage polarization and the in vivo study. a) Macrophage response induced by PEUU microfiber and cast degradation products. Primary BMMs were seeded into a 12 well plate and, after 7 days, were treated with 1:10 and 1:50 dilutions of PEUU microfiber and cast degradation products or with macrophage activation controls: IFN-γ + LPS (M1-like macrophages) and IL-4 (M2-like macrophages). After 16 h of incubation, stimulated macrophages were stained with one of the following primary antibodies: anti-F4/80 (pan-macrophage marker), iNOS (M1-like marker), and anti-Arginase1 and anti-Fizz1 (M2-like markers). b) Macrophage response induced by PEUU layer and wire scaffold morphology. BMMs were seeded onto the surface of 2 cm diameter sterile disks of either PEUU cast or microfiber layers and on PEUU microfiber sterile wires. After 7 days of differentiation, the expression of macrophage activation markers was evaluated by immunoblotting on macrophages seeded on PEUU disks, either cast or microfiber, and by immunolabeling on macrophages seeded on PEUU microfiber wires. Macrophage response was assessed using the following primary antibodies: iNOS (M1-like marker) and anti-Arginase1 and anti-Fizz1 (M2-like markers). c) Schematic of the in vivo study: a 2.5 cm incision was made between the scapulae of each animal following the cranial-caudal axis. The skin was closed with two interrupted sutures using one of the following materials: PEUU cast, PEUU microfiber, PGA, PDS, PPL.

notion that microstructure can be utilized to augment the performance of bioimplants as suture materials.[32,58]

Host response to biomaterials implantation was comparatively evaluated in a surgical wound rat model. The performance of PEUU microfiber wire with tailored structure and mechanics was compared to some of the most commonly adopted suture materials: PPL, PGA, and PDS. The analysis of the in vivo data included: gross evaluation (Figure 5), collagen synthesis (Figure 6), macrophages infiltration and polarization (Figure 7), uniaxial mechanics of the suture material (Figure 8), and biaxial mechanics of the tissue surrounding the suture material (Figure 9).

Despite the differences between the wires used, there was no macroscopic evidence of fibrosis nor differences in the epithelialization process among the groups 30 days after surgery (Figure 5). This can be considered a positive outcome, given that the control groups represented a state-of-the-art suture material for clinical use. As expected, due to its rapid degradation rate, PGA sutures started to disappear by the second week of the in vivo experiment and were fully absorbed at the time of sacrifice.

Both microfiber-based and monofilament suture wires, absorbable and nonabsorbable, entirely supported healing and showed good knot security without any necrosis or adverse reaction.

However, tissue cross-sections underneath the wound showed significant differences between groups in terms of collagen deposition (Figure 6 and Figure S5, Supporting Information) and inflammatory infiltrate (Figure 7). The PGA and PDS groups showed less collagen content and higher granulomatous tissue formation along the area of implanted suture materials compared to the healthy control. A definitive explanation for this more pronounced inflammatory response and lower collagen content remains unknown. However, differences noted can be related to four domains: suture material compositions, microarchitectures, mechanical properties, and degradation products.[59,60] For example, the PGA group showed less constructive remodeling. Consistently, local production of glycolic acid[59] is associated with an undesired inflammatory response.[61]

In contrast to the PGA and PDS groups, the histological observation of the PEUU microfiber group showed collagen content comparable to the healthy control and sparse inflammatory infiltrate.

Furthermore, the results of this study showed that constitutive remodeling is associated with phenotypic differences in macrophages. In particular, the PEUU cast group showed a higher number of M1 macrophages (Figure 7d); conversely, the PEUU microfiber group induced an M2-like phenotype (Figure 7c). While the two suture wires have the same chemistry, the delayed macrophagic switch in the PEUU cast group may result from different material degradation rates due to the differences in the microstructure. The animals treated with PEUU microfiber wires also exhibited a higher M2:M1 macrophage phenotype ratio than the ratio measured for the other suture materials (Figure 7b). It has been amply demonstrated that both M1 and M2 macrophages are required for an appropriate repair of damaged tissues; however, a higher M2:M1 ratio in the proximity of the bioimplant toward the early post-implantation period (up to 30 days) defines the milieu and is predictive of downstream functional tissue remodeling. In contrast to an early transition to the M2 phenotype, a prolonged presence of M1 macrophages is linked to a large amount of pro-inflammatory signaling, fibrosis, scarring, and ECM breakdown.[7–9,33,37]

The findings of the presented study can be considered a step forward in understanding how the topological cues of bioimplants, such as bioengineered suture wires with a tailored microarchitecture, can have an immunoregulatory role and influence the tissue remodeling outcomes.

Besides cellular infiltration, the proper choice of the suture material has broad implications in tissue repair, and it is a function of several other factors, including material mechanical properties. In general, the biomechanics of the material should be adequate to match the physical tissue demand and ideally restore the native mechanics and the physiological mechanotransduction of the treated area.

To investigate how material degradation and tissue remodeling affect suture material mechanical properties, uniaxial tensile test was conducted before and after the in vivo test (Figure 8).

After 30 days, rats were sacrificed, suture wires were gently removed from the wound site and collected for the mechanical evaluations. PGA sutures were fully degraded. In contrast, PDS and PEUU microfiber entirely preserved their mechanical properties after the implantation. PEUU microfiber initial tensile modulus and ultimate tensile strength were statistically equivalent to those shown by the rat skin control group showing the ability of these materials to reduce the risk of mechanical mismatch.[62] Interestingly, the PEUU cast wires and the PPL groups showed drastic changes in the mechanical properties before and after the in vivo implantation. This effect is most probably related to the host environment. However, the underline mechanism of such modification is still poorly understood. Even though sutures are the most used bioimplant, only a few works analyze the impact of the in vivo incubation on the suture materials.[63] Despite this phenomenon is relevant to the clinical use of sutures, it was behind the scope of this report and will be the object of further and deeper investigations.

To assess how the material implantation affected the mechanics of the treated site, the biaxial test was conducted on the explants (Figure 9). Results did not show any difference between the explants and the healthy rat skin control group. This was corroborated by the histological evaluation that did not show any relevant fibrotic area for all groups.

Several limitations can be listed and discussed in this study. First, to decouple the effects of the wire microarchitecture by the mechanical properties of the PEUU microfiber wire, a microfiber wire showing mechanical properties closer to the sutures available on the market should be included as a control. Second, only a few markers were used to determine the macrophage phenotype in the in vitro and in vivo experiments. Third, due to the complexity of seeding macrophages on the surface of the suture wires, immunohistochemical assessment was preferred to immunoblotting. Fourth, the opacity of the polymeric, fibrous biomaterial did not allow for successful cell imaging of the PEUU layers. For this reason, the macrophagic markers were evaluated using immunoblotting. Fifth, a single time point was selected for the in vivo evaluation. Multiple time points would have improved our understanding of the time evolution of the biomaterials–host interaction. Sixth, while the in vivo test did not show any weakness in the structure of the tested materials, a proper mechanical knot security study was not performed. Seventh, utilizing the

current set-up of the mandrel-less apparatus, continuously producing multilayer microfiber wires is not possible. The fabrication of multilayer wires is based on the collection of microfiber onto a core target. Assuming a potential expansion of this device, more fabrication possibilities can be explored. Finally, the suture materials chosen as controls for this report represent a somewhat limited fraction of degradable and not degradable suture material present on the market.

4. Conclusions

This study introduces a novel mandrel-less fabrication methodology for polymeric wires, with a circular cross-section, unlimited length, and controllable microarchitecture. The use of this fabrication apparatus allows for the production of microfiber bundles with tunable ultrastructure and mechanical properties that can be used as suture materials and as tissue surrogates for tendon and ligaments repair.

The potential translational value of an engineered suture wire was comparatively assessed in vitro and in vivo. We can conclude that a microstructured wire with tailored-to-the-needs mechanical properties improved the macrophagic biological outcomes and showed favorable results in terms of constructive remodeling when compared to constructs with the same chemistry and bulk structure and with some of the most common suture materials.

Altogether, the results obtained in this work are consistent with previously reported data on macrophagic response to biomaterials topological cues,[12,32,33] and most importantly, they provided proof of concept on a small animal model that further extends this notion to the broad application of the medical textiles.

5. Experimental Section

Mandrel-Less Electrodeposition Apparatus: A schematic of the mandrel-less electrodeposition apparatus introduced in this work is provided in Figure 1a. The apparatus was consisted of a stainless steel polymer injector, a two-tower stage made of Delrin, and three motors (M1, M2, M3) located inside the two towers. Motors M1 and M2 independently controlled the rotation and velocity (ω_1 and ω_2) of two copper electrodes around a common axis. M3 was responsible for the speed and direction of the take-up unit hosted in tower one. Once the direct current voltage was provided to the two electrodes (V_G) and to the polymer injector (V_P), using voltage generators (Gamma High Voltage Research, Inc.), a voltage gap was created and, in the absence of a solid collecting target, the polymeric fibers were deposited in the physical gap between the two electrodes. Figure S1 in the Supporting Information shows the mandrel-less apparatus device prototype and examples of a microfiber rope.

Poly(esther urethane)Urea (PEUU) Microfiber-Based Suture Wire Fabrication: The processing method was based on the notion of mandrel-less deposition that was previously introduced in the seminal study by Spiaggia et al.[55] In this work, two static electrically charged electrodes with opposite and spaced tips had been used to induce the deposition of highly aligned microscopic fibers deposition. The microfibers macroscopically spanned the space between the electrodes creating macroscopic filaments in a range of 2–6 cm in length. The limitations of this work included the construct length and the microfiber arrangement that could not be controlled. In the current study, the same idea of electrodeposition on a volume suspended between two electrodes had been further expanded by the possibility to control, with independent motors, the rotation of the electrodes, and by the capacity to continuously collect polymer mass with a spool system during the fiber deposition process. More specifically, the microfiber wire fabrication started when the mandrel-less apparatus and the polymer needle were electrically connected to a power source, and the polymer solution flowed throughout the syringe. The generated voltage created an accumulation of electrical charges between the two facing, spaced-apart electrodes, and that caused microfibers to align along with the target, spacing from the distal end of the first electrode to the one of the second. Thereby a nascent microfiber rope was formed. Once the first guide was produced, the take-up unit would be activated, and the fiber collection spool would draw the microfiber wire away from the first fiber collection. Different microfiber arrangements could be obtained by changing the electrode rotation velocities around their common axis. PEUU was used to fabricate the microfiber wires used in this study and was synthesized as previously described.[64] The PEUU polymer was dissolved in a 12% w/v hexafluoro isopropanol (HFIP, Oakwood Chemical) solution. Polymer voltage was 10 kV, and the polymer flow rate was 3 mL h^{-1}. Target electrode voltages were −2 kV. Polymer needle-electrodes gap and electrode gap were both equal to 5 cm (Figure 1a). Samples utilized for the mechanical characterization were fabricated using the parameters shown in Table 1. Five different processing configurations were tested to assess the capacity of the deposition apparatus to control fiber arrangement at the mesoscopic level. Polymeric microfiber orientation was dictated by the correlation between electrode rotational speed and direction. For instance, the same rotational speed and different electrode rotational directions allowed the fiber deposition to follow the rotational axis (Figures 1e and 2a). The multilayer configurations were obtained by alternating deposition stages with different electrode rotational directions, so that different layers of microfibers with different main orientation angles could form an engineered construct at the macroscopic scale (Figure 1e and Figure S3, Supporting Information).

One of the objectives of this study was to evaluate the impact of the suture wire microarchitecture on the host response. The effects of the PEUU microfiber wire were investigated in vitro on the macrophage polarization, and in vivo on the macrophagic response and on the tissue remodeling (Figure 10b,c). For these experiments, the $\omega_1 = 30$ rpm $-\omega_2 = 30$ rpm configuration was tested. To obtain a long PEUU microfiber wire, the velocity of the spool mechanism (υ_{spool}) was set at 2 cm min^{-1}, the polymer voltage was 10 kV, and the target electrode voltages were −2 kV and the polymer flow rate was 3 mL h^{-1}. A deposition time of 20 min was corresponded to a round cross-sectioned rope of 32 cm in length with a diameter of 800 ± 250 µm (Figure S1e,f, Supporting Information). The characteristics of this wire allowed to match the properties of the treated organ, tailoring the mechanics and the microarchitecture of the construct to those showed by the rat skin.

A cast PEUU wire (PEUU cast) was used as the control group for the topological and mechanical characterization (Figure 1e,f) and the in vivo experiments (Figures 5 and 10c). PEUU cast wire was obtained injecting a 12% w/v PEUU solution in a polytetrafluoroethylene tube, with a 2.5 mm internal diameter, dried at room temperature in a fume hood for 48 h, and finally manually extruded. The wire obtained was a round cross-sectioned rope of 27 cm length with a diameter of 670 ± 170 µm. The PEUU cast wire was used to directly compare a material characterized by the same chemistry but without microfiber microstructure.

The PEUU microfiber and cast wires were suitable for different sterilizing procedures, including ethanol bath, ethylene oxide, and UV irradiation. In this work, the PEUU microfiber and cast wires were sterilized with three sequential washing in 70% ethanol solution of 15 min each. Next, samples were washed three times for 15 min in sterile phosphate-buffered saline (PBS) solution and finally exposed to UV light for 20 min.

In Silico Characterization of the Electric Study: To elucidate the electrodeposition mechanism, the electric field during the fabrication was modeled with COMSOL Multiphysics 5.2 software (COMSOL AB, Stockholm, Sweden). The 2D and 3D model sizes were 1 m^2 and 1 m^3, respectively. To reproduce the experimental set-up, the distance between the polymer needle and the electrodes and the mutual distance between the two electrodes were modeled as equal to 5 cm. An 18 Gauge needle and two 10 mm long cylindrical electrodes with a diameter of 0.45 mm were also modeled and included in the analysis (Figure 1c,d). The following built-in materials were selected from the software library for the electrodes DIN: Cu-ETP/UNS: C11000, and for the polymer needle: DIN: Al99.5/UNS:

A91050. *Air* was set as the medium for the space surrounding the needle and the electrodes. The relative permittivity for *Air* was manually set equal to 1.00059 while 10^{30} was assigned for both needle and electrodes. Conservation of electric charge was set as boundary condition. The applied voltages were equal to −2 and 10 kV for the electrodes and the needles, respectively. A physics-controlled meshing sequence with an extra fine mesh resolution was used for all the objects: in total, 129 179 tetrahedral elements (*CTETRA*) were utilized for the 3D analysis, and 35 724 triangular elements (*CTRIA6*) for the 2D analysis. A single stationary step using COMSOL solver "*sol1*" was utilized. A comprehensive analysis of the simulation results is provided as supplementary materials (Figure S2, Supporting Information).

Scanning Electron Microscopy and Fiber Analysis: Surface characteristics of the PEUU microfiber suture wires were evaluated by SEM. The samples were sputter-coated with 5 nm of gold-palladium (Sputter Coater 108 auto, Cressington Scientific Instruments) and imaged using a JEM-6335F SEM (Jeol) at a working distance of 8 mm and magnifications of 100X (Figure 1e) and 1000X (Figure 2a). Seven randomly chosen images were selected for each of the five scaffold groups. The sample visual inspection was coupled with a complete fiber network topology analysis. Fiber orientation index, orientation angle, diameter, pore size, and porosity were quantified with a custom-made algorithm previously developed with MATLAB (The Math-Works).[29]

PEUU Cast and Microfiber Layer Preparation: PEUU layers were used for the in vitro assessment of inflammatory activity on macrophages. For microfiber and cast layer fabrications, PEUU polymer was dissolved 12% w/v in HFIP. PEUU microfiber layer was fabricated as previously described in D'Amore et al.[65] A steel cylinder (114 mm diameter) was used as a collector for the electrodeposition. The cylinder was charged at −4 kV and was rotated at 750 rpm while it was translated at 0.15 cm min^{-1}. The polymer solution flow rate was 20 mL h^{-1}, the needle was set at 10 cm from the target and charged at 13 kV. The deposition time for the microfiber layer was 20 min. At the end of the process, the scaffold showed an average thickness of 40 ± 20 µm. The PEUU microfiber layer was dried at room temperature in a fume hood overnight. PEUU cast layer was obtained by pouring 4 mL of 12% w/v polymer solution onto a clean 13 cm diameter Delrin container with a flat surface. The cast layer was finally dried overnight, at room conditions, in a fume hood and had an average thickness of 30 ± 7 µm. The final products were used to obtain the PEUU degradation products and as the substrate for macrophage differentiation.

The disk shape samples used for the in vitro tests were obtained by cutting PEUU microfiber and cast layers with a 2 cm diameter surgical puncher. The disks were sterilized with three sequential washing in 70% ethanol solution of 15 min each. Next, samples were washed three times for 15 min in sterile PBS solution and finally exposed to UV light for 20 min.

In Vitro Accelerated Hydrolysis of PEUU Cast and Microfiber Layers: PEUU cast and microfiber layers were hydrolyzed using a well-established accelerated hydrolysis method.[9] Both layers were cut into 1 × 1 cm pieces, weighed, and placed in a 50 mL conical tube. The samples were hydrolyzed in a 6.7% w/v 3 M HCl solution at 37 °C and shaken at 50 rpm for 30 days. The solubilized products released by hydrolysis were neutralized to pH 7.0 with 10 M NaOH. The resulting solutions were dialyzed for 24 h with a 0.1–0.5 kD membrane (Float-A-LyzerG2 Dialysis Device, Fisher Scientific). The resulting PEUU degradation products were used to treat the macrophage culture.

Animal and Experimental Procedures: The animal work was conducted under protocol 19116188 (evaluation of host response to suture materials). All procedures were approved by and performed according to the University of Pittsburgh's Institutional Animal Care and Use Committee (IACUC). Female C57BL/6 mice (Jackson Laboratories) and female Sprague Dawley rats (Charles River Laboratories) were used for the in vitro characterization and the in vivo assessment, respectively.

Bone Marrow-Derived Macrophages (BMMs) Isolation and Culture: Primary BMMs were isolated as previously described.[66] Briefly, female 6 to 8 weeks old C57BL/6 mice were euthanized via CO_2 inhalation and cervical dislocation. Femurs, tibia, and fibula were harvested and washed three times in complete macrophage medium consisting of 10% fetal bovine serum (Invitrogen), 10% L929 supernatant, 10×10^{-3} M nonessential amino acids (Gibco), 10×10^{-3} M 4-(2-hydroxyethyl)-1-piperazineethanesulfonic acid (Gibco), 2×10^{-3} M L-glutamine (Gibco), 100 U mL^{-1} penicillin (Gibco), 100 mg mL^{-1} streptomycin (Gibco), and 0.1% β-mercaptoethanol in Dulbecco's modified Eagle medium high glucose (Gibco). In order to collect the cells, the medium was flushed through the medullary space of the harvested bones using a sterile syringe. For immunolabeling studies, BMMs were plated at 2×10^6 cells mL^{-1} into 6 well plates (Corning), and after 7 days were treated with PEUU degradation products (Figure 10a). For immunoblotting studies, BMMs were seeded at 5×10^6 cells mL^{-1} onto the surface of 2 cm diameter sterile disks of PEUU cast and PEUU microfiber. Disks were then positioned into a 12 well plate (Figure 10b). The medium was supplemented 24 h after seeding, BMMs were differentiated into macrophages for 7 days at 37 °C and 5% CO_2 with media changes every 48 h. BMMs were also seeded twice on PEUU microfiber sterile scaffold wire (1 cm long), with 20 µL of a 10×10^6 cells mL^{-1} suspension. The wires were maintained suspended into the well using two inert metallic pins for the entire duration of the experiment. After 7 days, macrophage expression was evaluated by immunolabeling (Figure 10b).

Macrophage Activation: At day 7, naïve macrophages were supplemented with 1:10 or 1:50 dilutions of PEUU cast degradation products, 1:10 or 1:50 dilution of PEUU microfiber degradation products, and 1 mL of the macrophage activation controls. These control solutions were composed as follows: complete media to induce M0 phenotype, 20 ng mL^{-1} IFN-γ (Peprotech) + 100 ng mL^{-1} LPS (Sigma Aldrich) to induce M1 phenotype, 20 ng mL^{-1} IL-4 to induce M2 phenotype. Treated macrophages were finally incubated for 16 h at 37 °C and 5% CO_2 (Figure 10a).

Immunolabeling of In Vitro Treated Macrophages: After 16 h of incubation, stimulated macrophages were washed with PBS and fixed for 20 min at room temperature with 4% paraformaldehyde (PFA, Sigma). PEUU microfiber seeded wires were collected, fixed in 10% neutral-buffered formalin (Sigma), and embedded in paraffin. Longitudinal sections of 5 µm in thickness were cut and mounted onto glass slides. To prevent nonspecific binding, fixed cells and wire sections were incubated in a blocking solution composed of PBS, 0.1% Triton-X (Sigma Aldrich), 0.1% Tween-20 (Sigma Aldrich), 4% goat serum (Sigma Aldrich), and 2% bovine serum albumin (BSA, Sigma Aldrich) for 1 h at room temperature. Blocking buffer was then removed, stimulated macrophages and sections were incubated at 4 °C for 16 h in a solution with one of the following primary antibodies: 1) monoclonal anti-F4/80 (Novus), at 1:200 dilution, as a pan-macrophage marker; 2) polyclonal anti-inducible nitric oxide synthase (iNOS, Abcam), at 1:100 dilution, as an M1-like marker, and, 3) anti-Arginase1 (Abcam), at 1:200 dilution, as an M2-like marker. Primary antibodies were removed, and after PBS washing, a solution of fluorophore-conjugated secondary antibodies, Alexa donkey anti-rabbit 488 or Alexa donkey anti-rat 488 (Invitrogen), was added to the appropriate well/section for 1 h at room temperature. The antibodies were then removed, cells were washed with PBS, and the nuclei were counterstained using 4′,6-diamidino-2-phenylindole (DAPI—Fluorescence Mounting Medium, Dako Omnis). Cytokine-activated macrophages were used to establish standardized exposure times (positive control), which were kept constant throughout the groups. Images of three independent fields of view were taken for each well using a fluorescence microscope (Axio Observer Z1 Fluorescence, Carl Zeiss) at 20X magnification. CellProfiler (Broad Institute) was used to quantify cell number within the images.

Immunoblotting of In Vitro Treated Macrophages: After 7 days of macrophage differentiation, the expression of their activation markers was evaluated on cell-seeded disks of either PEUU cast or PEUU microfiber and control groups, including macrophages seeded on multiwell plates. After 16 h of induced activation, stimulated macrophages and seeded PEUU disks were removed from the culture plates and washed with PBS. Samples were lysed in radioimmunoprecipitation assay buffer supplemented with a protease inhibitor cocktail (Sigma Aldrich). Lysates were then quantified using bicinchoninic acid (Bio-Rad). Western blots were performed loading 10 µg of protein in each well in three biological replicates. Protein samples were diluted 1:1 with 2X Laemmli buffer (Bio-Rad) containing 5% β-mercaptoethanol (Gibco) before being loaded on 20% polyacrylamide pre-cast gel (MiniPROTEAN TGX, Bio-Rad) and run at 150 V for

≈45 min in *tris*-glycine running buffer. The wet transfer was performed using polyvinylidene difluoride membranes (Bio-Rad) in *tris*-glycine transfer buffer with 20% methanol at 350 mAmp on ice. After 45 min, membranes were removed from the transfer chamber, washed for 10 min in *tris*-buffered saline, 0.1% Tween 20 (TBST), and blocked for 1 h in TBST with 5% BSA. After blocking, membranes were incubated overnight at 4 °C with: 0.1 mg mL^{-1} mouse-anti-β-actin (Santa Cruz Biotechnologies), 0.1 mg mL^{-1} rabbit-anti-arginase 1 (Abcam), or 0.1 mg mL^{-1} rabbit-anti-iNOS (Thermo Fisher). Following the primary antibody incubation, membranes were washed three times in TBST and subsequently incubated for 1 h at room temperature with goat-anti-rabbit horseradish peroxidase (HRP) conjugated antibodies (Dako Omnis Affinity Purified; Agilent) that were diluted 1:1000 in TBST with 5% BSA. Membranes were then washed three times with TBST, incubated in a chemiluminescent substrate (Clarity ECL Substrate; Bio-Rad) for 5 min, and, subsequently, imaged (ChemiDoc Touch; Bio-Rad). Acquired images were analyzed using NIH-ImageJ (Rasband, W.S., ImageJ, U. S. National Institutes of Health, Bethesda, Maryland, USA, https://imagej.nih.gov/ij/), groups were normalized to the appropriate loading controls. Densitometry results were averaged across the replicates, and their means were compared.

In Vivo Studies and Surgical Procedures: 2 months old female Sprague–Dawley rats ($n = 15$) were used to evaluate the host response to suture materials. Animals were anesthetized using 1–3% inhaled isoflurane until signs of consciousness. The hair overlying the dorsum of the animals is removed, the animals were placed prone on a warming pad while receiving inhaled isoflurane. The skin was cleansed using Betadine and ethanol and allowed to dry. A 2.5 cm incision was made between the scapulae over the craniocaudal direction (Figure 10c). The wound closure was carried out through tissue apposition and two interrupted sutures with three simple throws placed on each knot to assure the safety of the suture. A simple interrupted pattern was commonly used to treat surgical incisions on the skin. This pattern had some advantages, including precise reconstruction of the wound margins, precise tension control on each point, and less interference with the healing and blood supply.[67]

Rats were divided into five groups ($n = 3$ per group), and the wound closures were performed using one of the following materials (Figure 5):

1) PGA: USP size 3-0, ⌀ 250 µm (MV-J398-V, Oasis), a braided multifilament wire with a rapid absorption time, between 15 and 90 days.
2) PDS: PDS*II, USP size 2, ⌀ 600 µm (D8472, Ethicon), a monofilament wire with resorption time between 180 and 238 days.
3) PPL: USP size 3-0, ⌀ 250 µm (MV-8683-V, Oasis), a nonabsorbable monofilament wire.
4) PEUU cast: USP size 4, ⌀ ≈670 µm.
5) PEUU microfiber: USP size 5, ⌀ ≈800 µm.

The suture materials used were classified according to size, structure, and absorption time, referring to USP (United States Pharmacopoeia) standards (USP 41-NF36:2018). PEUU cast and PEUU microfiber wires were attached to a 21 Gauge stainless steel straight needle. The needles were previously sterilized using ethylene oxide. Immediately before performing the suture, the sterile PEUU microfiber/casted wire was inserted into the needle eye, and the double strand of the suture was pulled through the tissue.

All animals survived for 30 days post-surgery and were subsequently sacrificed via CO_2 inhalation and cervical dislocation.

Sample Preparation for Explants Evaluation: After 30 days, the hair from the dorsal skin was removed. Next, an area of 5 × 5 cm around the treated skin, including the underlying connective tissue, was harvested. The incision was divided in two parts, the cephalic side was used for the histological and immunohistochemical evaluation, while the caudal portion of the explant was retrieved for the biaxial mechanical test. To complement the characterization of the biaxial mechanics and assess the impact of the degradation in vivo, the suture materials were gently extracted from the sample collected and analyzed by the uniaxial mechanical test. Samples for the biaxial tests were flash-frozen for 1 min in isopentane (Sigma Aldrich) cooled in dry ice. Frozen samples were then stored at −80 °C for 1 week, thawed at 4 °C overnight, and rinsed in PBS for 1 h before testing.[68]

Histological Evaluation and Quantitative Collagen Assessment: Paraffin-embedded samples and healthy rat skin controls were transversely sectioned with a thickness of 5 µm and stained with Masson's trichrome to evaluate newly formed tissue, cellular infiltration, and fibrotic tissue area. Images of the entire sections were acquired using a brightfield microscope (Axio Observer Z1, Carl Zeiss) at 10X magnification (Figure 6a and Figure S5, Supporting Information). The histological inspection of the explants was coupled with quantitative measurements. More specifically, collagen density was measured within the wound area and compared to an equivalent tissue volume underneath the rat's healthy skin. NIH-ImageJ software for image analysis was utilized to crop the area among the region of interest and identify the sutured areas. A custom-made algorithm, developed in MATLAB, and described in ref. [30] was utilized to segment and quantify collagen-rich areas.

Immunolabeling of Tissue Sections: Paraffin-embedded samples, both PEUU microfiber wires seeded with BMMs (Figure 4d) and skin explants (Figure 7a), were transversely sectioned with a thickness of 5 µm. Slides were deparaffinized using xylene and ethanol gradients (100–70% EtOH). Immunofluorescence was performed to assess the macrophage population phenotypes. After deparaffinization, the slides were placed in citrate antigen retrieval buffer (10×10^{-3} M citric acid monohydrate, pH 6.0), microwaved at 900 W for 45 s, followed by 15 min at 180 W. The slides were then cooled in copper sulfate solution (10×10^{-3} M $CuSO_4$, 50×10^{-3} M ammonium acetate, pH 5.0) for 20 min. Sections were then rinsed three times in TBST solution and then incubated for 1 h at room temperature in blocking buffer containing 0.1% Triton-X 100, 0.1% Tween, 2% goat serum, and 1% BSA. The blocking buffer was then removed, and the sections were incubated overnight at 4 °C in a humidified chamber with 1:200 rabbit-anti-CD11b (Abcam), a pan-macrophage marker. Following overnight incubation, each slide was washed 2 min in TBST for three times. A 1:200 solution of goat-anti-rabbit HRP-conjugated secondary antibody (Dako Omnis) in blocking buffer was subsequently applied and microwaved at 360 W for 3 min in a humidified chamber and allowed to cool for 2 min before washing in TBST. After washing, sections were incubated with a 1:200 solution of red fluorescent HRP substrate (OPAL 570, Perkin Elmer) in 1X amplification diluent (Perkin Elmer) for 10 min and then washed in TBST. In order to remove anti-CD11b and anti-rabbit antibodies, sections were subjected to second antigen retrieval in citrate antigen retrieval buffer, followed by cooling copper sulfate solution, and blocked as previously described. For each slide, one section was incubated with a 1:200 solution of rabbit-anti-iNOS antibody (Invitrogen) in blocking buffer, and one section was incubated with a 1:200 solution of rabbit-anti-RELMα (PeproTech). Slides with the primary antibodies were then placed on a water bath and microwaved at 360 W for 3 min, followed by 2 min of cooling. Slides were then washed in TBST solution, and a 1:200 solution of goat-anti-rabbit HRP-conjugated secondary antibody was supplemented to the sections. Slides with secondary antibody solutions were then placed in the water bath and microwaved at 360 W for 3 min, followed by 2 min of cooling. After cooling, slides were washed in TBST. Each section was treated with a 1:200 solution of green fluorescent HRP substrate in 1X Amplification Diluent (OPAL 520, Perkin Elmer) and incubated in a dark humidified chamber for 10 min at room temperature. The sections were then washed in TBST and incubated with DAPI (Dako Omnis) nuclear counterstain for 5 min. Finally, the sections were washed with TBST and subsequently placed onto glass slides for imaging. A fluorescence microscope (Axio Observer Z1 Fluorescence, Carl Zeiss) was used to image the entire section for each sample. The images of the skin explant were acquired at 10X magnification, the PEUU microfiber wires were evaluated at 40X. CellProfiler was used to quantify cell numbers within the images.

Uniaxial Mechanical Test: Uniaxial tensile tests were performed using the MTS Insight Electromechanical Testing Systems with a load cell of 100 N. Samples were tested following the D2256/D2256M *Standard Test Method for Tensile Properties of Yarns by the Single-Strand Method*. Briefly, samples were subjected to a 0.75 N preload and strained at a speed of 25 mm min^{-1} until failure to determine the complete stress/strain curve. Before the uniaxial test, the sample diameters were measured using brightfield microscopy (Axio Observer Z1 Fluorescence, Carl Zeiss).

All the suture materials used for the in vivo study were tested before the implantation and immediately after the animal sacrifice. Three samples from each wire were evaluated before the implantation: two from the mid-extremities and one from the central part of the wires. For the PEUU cast and microfiber wires, the mechanical characterization was performed on long cables (≈29 cm in length) 24 h after the fabrication. After the in vivo implantation, the wires were gently removed from the rat skin and quickly rinsed in PBS. After the wire collection, the diameter of each wire was recorded, and the samples were tested. Rat dorsal skin between the scapulae was harvested and utilized as a control. The rat skin samples were cut with a dog bone-shaped puncher. Samples were oriented so that the longer direction was parallel to the spine of the animal.

Biaxial Mechanical Test: In order to determine the in-plane mechanical properties of rat skin, a custom-built biaxial stretching system was used. Samples were cut in a 10 × 10 mm square shape that was centered on the wound/suture line. Before affixing the samples for biaxial testing, the subcutaneous layer and panniculus carnosus were removed. Markers were placed on the corners of a squared area at the center of the sample and used to calculate the deformation gradient tensor. Tests were performed using a Lagrangian equi-stress control protocol, a maximum load of 250 kPa[68] was adopted to induce large deformations. Samples were preconditioned for 10 cycles of 30 s in PBS at room temperature. Data processing was performed, as previously described,[65] with a custom-made software developed in MATLAB using the post-conditioning, free float configuration was used as a reference.

Statistical Analysis: Statistical analysis was performed using SigmaPlot version 14.0 (Systat Software Inc.) and GraphPad Prism version 8 (GraphPad Software). The differences in the mean values between the groups were determined by paired *t*-test and one-way analysis of variance (ANOVA). Brown-Forsythe and Welch ANOVA was used to determine differences of the mean values between the groups within the uniaxial mechanical properties evaluation. When differences between the groups were found significant, statistical analysis was conducted with a post hoc Tukey honestly significant difference, Dunnett's T3 or Student-Newman-Keuls post hoc tests. All data were presented as mean ± standard error of the mean. The significance level was set at $p < 0.05$.

Supporting Information

Supporting Information is available from the Wiley Online Library or from the author.

Acknowledgements

The authors acknowledge Dr. Catalina Pineda Molina and Dr. Neill Turner for the insights and advice provided and the McGowan Institute for Regenerative Medicine Histology Laboratory. The authors also like to acknowledge Biorender (BioRender – https://app.biorender.com/) since icons and graphical abstract of this manuscript were made using this software. This work was funded by the Ri.MED Foundation 2019 research support "Development of novel biomaterials for tissue engineering strategies," by the Italian Ministry of Education, University and Research "PON Innovation and Research project—DOT1720429" and by the European Research Council CoG # 101002561 "BIOMITRAL."

Conflict of Interest

The authors declare no conflict of interest.

Data Availability Statement

The data that support the findings of this study are available from the corresponding author upon reasonable request.

Keywords

biofabrication, biomaterials host response, inflammation, macrophagic responses, medical textiles

Received: November 30, 2021
Revised: March 27, 2022
Published online:

[1] C. Dennis, S. Sethu, S. Nayak, L. Mohan, Y. Morsi, G. Manivasagam, *J. Biomed. Mater. Res., Part A* **2016**, *104*, 1544.
[2] F. Ahmed, I. A. Shaikh, T. Hussain, I. Ahmad, S. Munir, M. Zameer, *Pak. J. Nutr.* **2014**, *13*, 780.
[3] R. H. H. Tan, R. Bell, B. Dowling, A. Dart, *Aust. Vet. J.* **2003**, *81*, 140.
[4] I. Capperauld, *Clin. Mater.* **1989**, *4*, 3.
[5] J. M. Kümmerle, C. Fogle, in *Equine Surgery*, 5th ed. (Eds: J. Auer, J. Stick), W. B. Saunders, St Louis **2018**, pp. 255–280.
[6] J. Anderson, S. Cramer, in *Host Response to Biomaterials* (Ed: S. F. Badylak) Elsevier, New York **2015**, p. 13.
[7] B. N. Brown, R. Londono, S. Tottey, L. Zhang, K. A. Kukla, M. T. Wolf, K. A. Daly, J. E. Reing, S. F. Badylak, *Acta Biomater.* **2012**, *8*, 978.
[8] B. N. Brown, B. D. Ratner, S. B. Goodman, S. Amar, S. F. Badylak, *Biomaterials* **2012**, *33*, 3792.
[9] C. P. Molina, R. Giglio, R. M. Gandhi, B. M. Sicari, R. Londono, G. S. Hussey, J. G. Bartolacci, L. M. Q. Luque, M. C. Cramer, J. L. Dziki, *J. Immunol. Regener. Med.* **2019**, *3*, 13.
[10] a) W.-J. Li, R. L. Mauck, J. A. Cooper, X. Yuan, R. S. Tuan, *J. Biomech.* **2007**, *40*, 1686; b) S. B. Orr, A. Chainani, K. J. Hippensteel, A. Kishan, C. Gilchrist, N. W. Garrigues, D. S. Ruch, F. Guilak, D. Little, *Acta Biomater.* **2015**, *24*, 117.
[11] Z. Ma, M. Kotaki, R. Inai, S. Ramakrishna, *Tissue Eng.* **2005**, *11*, 101.
[12] A. D. Schoenenberger, H. Tempfer, C. Lehner, J. Egloff, M. Mauracher, A. Bird, J. Widmer, K. Maniura-Weber, S. F. Fucentese, A. Traweger, *Biomaterials* **2020**, *249*, 120034.
[13] A. Sensini, L. Cristofolini, *Materials* **2018**, *11*, 1963.
[14] A. D'Amore, S. K. Luketich, G. M. Raffa, S. Olia, G. Menallo, A. Mazzola, F. D'Accardi, T. Grunberg, X. Gu, M. Pilato, *Biomaterials* **2018**, *150*, 25.
[15] A. Capulli, L. MacQueen, S. P. Sheehy, K. Parker, *Adv. Drug Delivery Rev.* **2016**, *96*, 83.
[16] S. Panseri, C. Cunha, J. Lowery, U. Del Carro, F. Taraballi, S. Amadio, A. Vescovi, F. Gelain, *BMC Biotechnol.* **2008**, *8*, 39.
[17] M. S. Khil, S. R. Bhattarai, H. Y. Kim, S. Z. Kim, K. H. Lee, *J. Biomed. Mater. Res., Part B* **2005**, *72*, 117.
[18] A. E. Smit, R. D. Sanderson, "Yarn and a process for manufacture thereof." *U.S. Patent No. US8522520B2*, **2013**.
[19] W. E. Teo, W. He, S. Ramakrishna, *Biotechnol. J.* **2006**, *1*, 918.
[20] M. Yousefzadeh, M. Latifi, W. E. Teo, M. Amani-Tehran, S. Ramakrishna, *Polym. Eng. Sci.* **2011**, *51*, 323.
[21] F. Dabirian, Y. Hosseini, S. H. Ravandi, *J. Text. Inst.* **2007**, *98*, 237.
[22] M. B. Bazbouz, G. K. Stylios, *Eur. Polym. J.* **2008**, *44*, 1.
[23] U. Ali, Y. Zhou, X. Wang, T. Lin, *J. Text. Inst.* **2012**, *103*, 80.
[24] A. M. Afifi, S. Nakano, H. Yamane, Y. Kimura, *Macromol. Mater. Eng.* **2010**, *295*, 660.
[25] C. L. He, Z. M. Huang, X. J. Han, *J. Biomed. Mater. Res., Part A* **2009**, *89*, 80.
[26] X. Liao, M. Dulle, J. M. d. S. e Silva, R. B. Wehrspohn, S. Agarwal, S. Förster, H. Hou, P. Smith, A. Greiner, *Science* **2019**, *366*, 1376.
[27] A. S. Richard, R. S. Verma, *Mater. Sci. Eng., C* **2021**, *128*, 112334.
[28] P.-A. Mouthuy, N. Zargar, O. Hakimi, E. Lostis, A. Carr, *Biofabrication* **2015**, *7*, 025006.

[29] A. D'Amore, J. A. Stella, W. R. Wagner, M. S. Sacks, *Biomaterials* **2010**, *31*, 5345.
[30] A. D'Amore, M. Fazzari, H.-B. Jiang, S. K. Luketich, M. E. Luketich, R. Hoff, D. L. Jacobs, X. Gu, S. F. Badylak, B. A. Freeman, *Tissue Eng., Part A* **2018**, *24*, 889.
[31] M. Kara, P. P. Kondiah, T. Marimuthu, Y. E. Choonara, *Carbohydr. Polym.* **2021**, *261*, 117860.
[32] R. Sridharan, A. R. Cameron, D. J. Kelly, C. J. Kearney, F. J. O'Brien, *Mater. Today* **2015**, *18*, 313.
[33] B. N. Brown, S. F. Badylak, *Acta Biomater.* **2013**, *9*, 4948.
[34] F. Alshomer, A. Madhavan, O. Pathan, W. Song, J. M. Seitz, M. Durisin, J. Goldman, J. W. Drelich, *Adv. Healthcare Mater.* **2015**, *4*, 1915.
[35] a) S. Chen, B. Liu, M. A. Carlson, A. F. Gombart, D. A. Reilly, J. Xie, *Nanomedicine* **2017**, *12*, 1335; b) N. M. Lee, C. Erisken, T. Iskratsch, M. Sheetz, W. N. Levine, H. H. Lu, *Biomaterials* **2017**, *112*, 303; c) Q. P. Pham, U. Sharma, A. G. Mikos, *Tissue Eng.* **2006**, *12*, 1197.
[36] F. Selvi, S. Cakarer, T. Can, S. İ. K. Topcu, A. Palancioglu, B. Keskin, B. Bilgic, M. Yaltirik, C. Keskin, *J. Istanbul Univ. Fac. Dent.* **2016**, *50*, 35.
[37] S. Chen, J. A. Jones, Y. Xu, H.-Y. Low, J. M. Anderson, K. W. Leong, *Biomaterials* **2010**, *31*, 3479.
[38] C. E. Witherel, D. Abebayehu, T. H. Barker, K. L. Spiller, *Adv. Healthcare Mater.* **2019**, *8*, 1801451.
[39] Y. Kawakami, K. Nonaka, N. Fukase, A. D'Amore, Y. Murata, P. Quinn, S. Luketich, K. Takayama, K. G. Patel, T. Matsumoto, *Acta Biomater.* **2021**, *121*, 275.
[40] W. L. Lim, L. L. Liau, M. H. Ng, S. R. Chowdhury, J. X. Law, *Tissue Eng. Regener. Med.* **2019**, *16*, 549.
[41] A. H. Khalighi, B. V. Rego, A. Drach, R. C. Gorman, J. H. Gorman, M. S. Sacks, *Ann. Biomed. Eng.* **2019**, *47*, 60.
[42] K. Zuo, T. Pham, K. Li, C. Martin, Z. He, W. Sun, *J. Mech. Behav. Biomed. Mater.* **2016**, *62*, 607.
[43] a) J. Seeburger, M. Rinaldi, S. L. Nielsen, S. Salizzoni, R. Lange, M. Schoenburg, O. Alfieri, M. A. Borger, F. W. Mohr, A. Aidietis, *J. Am. Coll. Cardiol.* **2014**, *63*, 914; b) A. Colli, D. Adams, A. Fiocco, N. Pradegan, L. Longinotti, M. Nadali, D. Pandis, G. Gerosa, *Ann. Cardiothorac. Surg.* **2018**, *7*, 812.
[44] U. O. von Oppell, F. W. Mohr, *Ann. Thorac. Surg.* **2000**, *70*, 2166.
[45] L. Soletti, Y. Hong, J. Guan, J. J. Stankus, M. S. El-Kurdi, W. R. Wagner, D. A. Vorp, *Acta Biomater.* **2010**, *6*, 110.
[46] J. Dias, P. Granja, P. Bártolo, *Prog. Mater. Sci.* **2016**, *84*, 314.
[47] T. Xu, J. M. Miszuk, Y. Zhao, H. Sun, H. Fong, *Adv. Healthcare Mater.* **2015**, *4*, 2238.
[48] E. Smit, U. Bűttner, R. D. Sanderson, *Polymer* **2005**, *46*, 2419.
[49] J. He, Y. Zhou, K. Qi, L. Wang, P. Li, S. Cui, *Fibers Polym.* **2013**, *14*, 1857.
[50] a) H. Yan, L. Liu, Z. Zhang, *Mater. Lett.* **2011**, *65*, 2419; b) A. Mondal, R. Borah, A. Mukherjee, S. Basu, M. Jassal, A. K. Agrawal, *J. Appl. Polym. Sci.* **2008**, *110*, 603; c) F. Hajiani, A. A. Jeddi, A. Gharehaghaji, *Fibers Polym.* **2012**, *13*, 244.
[51] N. Bhardwaj, S. C. Kundu, *Biotechnol. Adv.* **2010**, *28*, 325.
[52] S. Yang, K.-F. Leong, Z. Du, C.-K. Chua, *Tissue Eng.* **2001**, *7*, 679.
[53] T. B. Wissing, V. Bonito, E. E. van Haaften, M. van Doeselaar, M. M. Brugmans, H. M. Janssen, C. V. Bouten, A. I. Smits, *Front. Bioeng. Biotechnol.* **2019**, *7*, 87.
[54] W. Teo, S. Ramakrishna, *Nanotechnology* **2005**, *16*, 1878.
[55] G. Spiaggia, A. Adamo, G. Coyan, W. R. Wagner, A. D'Amore, *Struct. Heart* **2019**, *3*, 70.
[56] C. Chu, in *Biotextiles as Medical Implants* (Eds: M. W. King, B. S. Gupta, R. Guidoin) Elsevier, New York **2013**, pp. 231–273.
[57] N. Mehrban, C. P. Molina, L. M. Quijano, J. Bowen, S. A. Johnson, J. Bartolacci, J. T. Chang, D. A. Scott, D. N. Woolfson, M. A. Birchall, *Acta Biomater.* **2020**, *111*, 141.
[58] a) P. C. Bota, A. M. Collie, P. Puolakkainen, R. B. Vernon, E. H. Sage, B. D. Ratner, P. S. Stayton, *J. Biomed. Mater. Res., Part A* **2010**, *95*, 649; b) H. Cao, K. Mchugh, S. Y. Chew, J. M. Anderson, *J. Biomed. Mater. Res., Part A* **2010**, *93*, 1151.
[59] B. D. Ulery, L. S. Nair, C. T. Laurencin, *J. Polym. Sci., Part B: Polym. Phys.* **2011**, *49*, 832.
[60] M. Yaltirik, K. Dedeoglu, B. Bilgic, M. Koray, H. Ersev, H. Issever, O. Dulger, S. Soley, *Oral Dis.* **2003**, *9*, 284.
[61] a) J. Otto, M. Binnebösel, S. Pietsch, M. Anurov, S. Titkova, A. Öttinger, M. Jansen, R. Rosch, D. Kämmer, U. Klinge, *J. Invest. Surg.* **2010**, *23*, 190; b) K. Ceonzo, A. Gaynor, L. Shaffer, K. Kojima, C. A. Vacanti, G. L. Stahl, *Tissue Eng.* **2006**, *12*, 301.
[62] A. Carnicer-Lombarte, D. G. Barone, I. B. Dimov, R. S. Hamilton, M. Prater, X. Zhao, A. L. Rutz, G. G. Malliaras, S. P. Lacour, C. E. Bryant, *Biorxiv* **2019**, 829648.
[63] a) D. Greenwald, S. Shumway, P. Albear, L. Gottlieb, *J. Surg. Res.* **1994**, *56*, 372; b) D. Stankevicius, J. Jonusas, V. Zalgeviciene, S. Ryliskis, *Cureus* **2019**, *11*.
[64] J. Guan, M. S. Sacks, E. J. Beckman, W. R. Wagner, *Biomaterials* **2004**, *25*, 85.
[65] A. D'Amore, T. Yoshizumi, S. K. Luketich, M. T. Wolf, X. Gu, M. Cammarata, R. Hoff, S. F. Badylak, W. R. Wagner, *Biomaterials* **2016**, *107*, 1.
[66] a) M. Englen, Y. Valdez, N. Lehnert, B. Lehnert, *J. Immunol. Methods* **1995**, *2*, 281; b) B. M. Sicari, J. L. Dziki, B. F. Siu, C. J. Medberry, C. L. Dearth, S. F. Badylak, *Biomaterials* **2014**, *35*, 8605.
[67] J. A. Auer, J. A. Stick, *Equine Surgery-E-Book*, Elsevier Health Sciences, Amsterdam **2018**.
[68] S. Chen, A. N. Annaidh, S. Roccabianca, *Biomech. Model. Mechanobiol.* **2020**, *19*, 275.